Atmospheric
Measurement
Techniques
Discussions

Real-time UV-Index retrieval in Europe using Earth Observation based techniques and validation against ground-based measurements

Panagiotis G. Kosmopoulos[1], Stelios Kazadzis[2], Alois W. Schmalwieser[3], Panagiotis I. Raptis[1], Kyriakoula Papachristopoulou[1], Ilias Fountoulakis[1,4], Akriti Masoom[5], Alkiviadis F. Bais[6], Julia Bilbao[7], Mario Blumthaler[8], Axel Kreuter[8,9], Anna Maria Siani[10], Kostas Eleftheratos[11], Chrysanthi Topaloglou[5], Julian Gröbner[2], Bjørn Johnsen[12], Tove Svendby[13], Jose Manuel Vilaplana[14], Lionel Doppler[15], Ann R. Webb[16], Marina Khazova[17], Hugo De Backer[18], Anu Heikkilä[19], Kaisa Lakkala[20], Janusz Jaroslawski[21], Charikleia Meleti[5], Henri Diémoz[4], Gregor Hülsen[2], Barbara Klotz[8], John Rimmer[16], Charalampos Kontoes[1]

[1]National Observatory of Athens, Athens, Greece
[2]Physikalisch-Meteorologisches Observatorium Davos, World Radiation Center, Davos Dorf, Switzerland
[3]University of Veterinary Medicine, Vienna, Austria
[4]Environmental Protection Agency of Aosta Valley, Aosta, Italy
[5]Indian Institute of Technology Roorkee, India
[6]Aristotle University of Thessaloniki, Greece
[7]Valladolid University, Valladolid, Spain
[8]Innsbruck Medical University, Innsbruck, Austria
[9] Luftblick OG, Innsbruck, Austria
[10]Sapienza University of Rome, Rome, Italy
[11]National and Kapodistrian University of Athens, Athens, Greece
[12]Norwegian Radiation and Nuclear Safety Authority, Bærum, Norway
[13]Norwegian Institute for Air Research, Bærum, Norway
[14]National Institute for Aerospace Technology, Torrejón de Ardoz, Spain
[15]German Weather Service, Offenbach, Germany
[16]University of Manchester, Manchester, UK
[17]Public Health England, London, UK
[18]Royal Meteorological Institute of Belgium, Bruxelles, Belgium
[19]Finnish Meteorological Institute, Helsinki, Finland
[20]Finnish Meteorological Institute, Sodankylä, Finland
[21]Institute of Geophysics, Polish Academy of Sciences, Warsaw, Poland

Correspondence to: P.G. Kosmopoulos (pkosmo@noa.gr)

Abstract. This study introduces an Earth observation (EO)-based system which is capable of operationally estimating and continuously monitoring the ultraviolet index (UVI) in Europe. The UVIOS (i.e. UV-Index Operating System) exploits a synergy of radiative transfer models with high performance computing and EO data from satellites (Meteosat Second Generation and Meteorological Operational Satellite-B), and retrieval processes (Tropospheric Emission Monitoring Internet Service, Copernicus Atmosphere Monitoring Service and the Global Land Service). It provides a near-real-time now-casting

Atmospheric
Measurement
Techniques
Discussions

39   and short-term forecasting service for UV radiation over Europe. The main atmospheric inputs for the UVI simulations include

40   ozone, clouds and aerosols while the impacts of ground elevation and surface albedo are also taken into account. The UVIOS

41   output is the UVI at high spatial and temporal resolution (5 km and 15 minutes, respectively) for Europe (i.e. 1.5 million pixels)

42   in real-time. The UVI is empirically related to biologically important UV dose rates and the reliability of this EO-based solution

43   was verified against ground-based measurements from 17 stations across Europe. Stations are equipped with spectral,

44   broadband or multi-filter instruments and cover a range of topographic and atmospheric conditions. A period of over one year

45   of forecasted 15-min retrievals under all sky conditions were compared with the ground–based measurements. UVIOS

46   forecasts were within ±0.5 of measured UVI for at least 70% of the data compared at all stations. For clear sky conditions the

47   agreement was better than 0.5 UVI for 80% of the data. A sensitivity analysis of EO inputs and UVIOS outputs was performed

48   in order to quantify the level of uncertainty in the derived products, and to identify the covariance between the accuracy of the

49   output and the spatial and temporal resolution, and the quality of the inputs. Overall, UVIOS slightly overestimated UVI due

50   to observational uncertainties in inputs of cloud and aerosol. This service will hopefully contribute to EO capabilities and will

51   assist the provision of operational early warning systems that will help raise awareness among European Union citizens of the

52   health implications of high UVI doses.

53   **Keywords.** Ultraviolet Index; Earth Observation; Radiative Transfer; High Performance Computing; Clouds; Aerosols;

54   Ozone; Solar Zenith Angle; Ground Elevation; Surface Albedo

55   **1 Introduction**

56   Human exposure to ultraviolet (UV) radiation has both beneficial and harmful effects (Juzeniene et al., 2011; Lucas et al.,

57   2006). Overexposure to UV radiation (UVR) has a number of implications, such as the acute response of erythema, the risk of

58   skin cancer and a number of eye diseases (snow blindness, cataract). Nevertheless, exposure to solar UVB radiation is the main

59   mechanism for the synthesis of Vitamin D in the human skin (Holick, 2002; Webb and Engelsen, 2008; Webb et al., 2011).

60   Low levels of the Vitamin D are associated with depression of the immune system and there is evidence that is linked to a

61   number of medical implications (Lucas et al., 2015).

62   The UV index was introduced by WHO/WMO in 1994 (WMO, 1995), as a simple method of informing the general public

63   about the erythema effective (sun-burning) UV. It is a unitless, scaled version of erythemally-weighted UV determined by

64   multiplying the erythema weighted irradiance (in W/m^2) by 40 m^2/W (Fioletov et al., 2010 ; Vanicek et al., 2000; WHO, 2002).

65   The response of UV radiation to climatic changes is of great concern (Bais et al., 2019; Bais et al., 2018; McKenzie et al.,

66   2011). According to the latest work of Bais et al. (2019) greater values of UV are expected by the end of 21st century, relative

67   to the present decade, at low latitudes, while at higher latitudes UV will decrease but these projections are associated with

68   high uncertainty (up to 30%).

69   There are many factors affecting UV irradiance reaching Earth's surface (Kerr and Fioletov, 2008). The dependence of UV

70   irradiance on astronomical and geometrical parameters is generally well understood, and in many cases the changes are

71   periodical (e.g. (Blumthaler et al., 1997; Gröbner et al., 2017; Larkin et al., 2000; Seckmeyer et al., 2008)). Atmospheric gases

72   play a crucial role in attenuating UV irradiance, with O_3 being the main absorber in the UVB (Bais et al., 1993), and NO_2 being

73   the main absorber in the UV-A (e.g. Cede et al. (2006)) spectral region. Aerosols are another important parameter controlling

74   UV irradiance levels at the surface (e.g. Kazadzis et al. (2009b)). Aerosol optical depth (AOD) that quantifies the attenuation

75   of the direct solar beam by aerosols is a parameter varying with wavelength, as well as single scattering albedo (SSA), which

76   determines the scattering ratio to total extinction. Several recent studies based on incoming UV irradiance measurements or

77   calculations reveal the enhanced absorption by aerosols in the UV relative to the visible spectral range. They show the

78   importance of using SSA in the UV spectral region, instead of interpolating SSA at visible wavelengths to the UV, or directly

79   using SSA at visible wavelengths, options that systematically overestimate UV irradiance (Corr et al., 2009; Fountoulakis et

80   al., 2019; Kazadzis et al., 2016; Mok et al., 2018; Raptis et al., 2018).

81   All the aforementioned parameters are particularly important under cloud free conditions. The cloudy sky complicates the

82   propagation of solar radiation, predominantly in the troposphere, through multiple cloud - radiation interactions. Nonetheless,

83   UVR is less affected than the total solar radiation by clouds (e.g. Badosa et al. (2014)). Bais et al. (1993) quantified that for

84   the city of Thessaloniki the change from 0 to 8/8 for cloud coverage corresponds to 80% reduction in the UVR and pointed

85   out that there is very low wavelength dependence of UVR attenuation by cloud cover. In other studies (Mayer et al., 1998;

86   Seckmeyer et al., 1996) the authors showed that although the transmittance of clouds does not vary significantly with

87   wavelength in the UV, clouds give a wavelength dependent effect to the diffuse component the surface UVR, due to the more

88   effective scattering and absorption of shorter UV wavelengths in the atmosphere acting on larger air masses. In cases of

89   partially cloudy sky but unobscured sun, UVR tends to be higher than in clear sky conditions (e.g. Badosa et al. (2014)), as is

90   the case for total solar radiation. For short timescale analysis the variability of UVR introduced by clouds should be considered.

91   A review of empirical studies of cloud effects on UVR is given by Calbó et al. (2005).

92   Solar UV irradiance at the surface increases with increasing surface albedo. This increment affects the UV radiant exposure,

93   which becomes crucial for outdoor human activities (Schmalwieser and Siani, 2018; Schmalwieser, 2020; Siani et al., 2008).

94   Measurements and computations of effective surface albedo for heterogeneous surfaces reveal its strong spectral dependence,

95   with snow-covered surfaces having significantly higher values of albedo for short wavelengths compared to total solar radiation

96   (Blumthaler and Ambach, 1988; Kreuter et al., 2014). Stronger enhancement of the UV relative to visible radiation over highly

97   reflective surfaces is also due to the more effective multiple scattering of shorter wavelengths in the atmosphere.

98   Any systematic changes in any of the parameters described in previous paragraphs have the potential to lead to changes for

99   UVR. These changes vary significantly throughout the globe and are attributed to different possible drivers (Bernhard and

100   Stierle, 2020; Fountoulakis et al., 2018; McKenzie et al., 2019). Fountoulakis et al. (2020a) gives a review of recent

101   publications concerning UV trends since 1990s, and associated factors, summarizing these as positive trends for South and

102   Central Europe and negative trends at higher latitudes, and recognizing the important role of aerosols and cloud coverage for

103 these trends in contrast to ozone. Findings from the same study demonstrated that the long – term changes of UV irradiance

104 recorded at four stations around Europe during the last two decades are mainly attributed to aerosols, cloud coverage and

105 surface albedo variations, with total ozone changes being of minor importance.

106 For the northern mid-latitudes Zerefos et al. (2012) showed that the long-term (1995-2006) positive trends in total ozone wasn't

107 enough to compensate for, let alone reverse, the UVB increase attributed to tropospheric aerosol decline (brightening effect).

108 Since 2007, a slowdown or even a possible turning point in the positive UVB trend was detected, which was attributed to the

109 continued upward trend in total ozone overwhelming the aerosol effect.By contrast, the long-term variability of UVB irradiance

110 over northern high latitudes was determined by ozone and not by aerosol trends, as shown by Eleftheratos et al. (2015) who

111 found a statistically significant negative trend of -3.9% per decade for the UVB irradiance during the time period 1999-2011,

112 from Ground-Based (GB) measurements at 7 stations. This was in agreement with statistically significant increase of

113 spaceborne measured total ozone by about 1.5% per decade (ozone recovery) for the same area. For Arctic regions changes in

114 snow cover have a great impact on UV trends according to Bernhard (2011), who concluded that the future Arctic UV climate

115 may be affected more by a warming climate changing the snow cover than changes in stratospheric ozone concentrations.

116 The continuous monitoring of the UV index is currently performed by about 160 stations from 25 countries around Europe

117 (Schmalwieser et al., 2017), with all monitoring instruments having the potential to provide other effective doses such as the

118 effective dose for the production of vitamin D in human skin (e.g. Fioletov et al. (2009)).

119 There are three types of instruments for UV irradiance measurements; those measuring the integral of UV irradiance

120 (broadband sensors) tailored to a specific response, narrow band instruments such as filter radiometers with coarse spectral

121 resolution, and instruments performing high resolution spectral measurements – the most versatile but most challenging and

122 least robust instruments. Concerning the current UV monitoring measurement accuracy; The European reference UV

123 spectroradiometer (QASUME) is a traveling instrument which provides a common standard through inter-comparison on-site

124 (Gröbner et al., 2005; Hülsen et al., 2016). During the period 2000-2005 the QASUME visited 27 spectroradiometers sites.

125 Out of the 27 instruments, 13 showed deviations of less than 4% relative to the QASUME reference spectroradiometer in the

126 UVB (for 15 instruments in the UVA) for solar zenith angles below 75°. The expanded relative uncertainty (coverage factor

127 k=2) of solar UV irradiance measurements by QASUME, for SZA smaller than 75° and wavelengths longer than 310 nm, was

128 4.6% in 2002 – 2014 (Gröbner and Sperfeld, 2005), and has been 2 % since 2014 (Hülsen et al., 2016). For broadband

129 instruments, the current instrument uncertainties are summarized in (Hülsen et al., 2020; Hülsen et al., 2008). In 2017, 75

130 broad-band instruments measuring the UV index, the UVB or/and the UVA irradiance participated in the solar UV broadband

131 radiometer comparison in Davos Switzerland. Using the instrument/user calibration factors, the differences between the

132 datasets by the broad-band instruments and the reference (QASUME) dataset were within ±5 % for 32 (43 %) of the instrument

133 datasets, ±10 % for 48 (64 %), and exceeded ±10 for % 27 (35 %).

134 Although ground-based monitoring of solar UVR is more accurate than satellite retrievals, ground based stations are sparse,

135 and the only way for continuous monitoring of the UVR on a global scale is through satellites. In recent decades instruments

136 on-board satellites have provided the necessary data for estimates of UV irradiance reaching the Earth surface on a global scale

Atmospheric
Measurement
Techniques
Discussions

137   (Herman, 2010) and hence satellite-derived UVR climatological studies have been conducted (Vitt et al., 2020; Verdebout,

138   2004). The satellite UV irradiance record started with the Total Ozone Mapping Spectrometer (TOMS) on-board Nimbus-7 in

139   1978 and continued with Ozone Monitoring Instrument (OMI) on-board NASA's satellite EOS-Aura. The OMI retrieval

140   algorithm for surface UVR estimates was based on the experience gained from TOMS (Levelt et al., 2018; Levelt et al., 2006).

141   The early surface UVR retrieval algorithms from satellite data didn't account for the enhanced aerosol absorption in the UV

142   spectral range, resulting in overestimated values (Krotkov et al., 1998). A lot of scientific effort has been put into correcting

143   the products (Arola et al., 2009). TROPOspheric Monitoring Instrument (TROPOMI) onboard Sentinel – 5 Precursor (Lindfors

144   et al., 2018) is the current satellite instrument that provides the surface UVR product on a daily basis with global coverage,

145   including 36 UVR parameters. As the aforementioned instruments were installed onboard polar orbiting satellites, providing

146   global spatial coverage, the temporal resolution of the data is daily since there are only one or two overpasses per day for every

147   point. Geostationary satellites provide continuous (in time) measurements over wide areas. The geostationary meteorological

148   satellites Meteosat monitor the full Earth Disk including Europe and their frequent data acquisition of rapidly changing

149   parameters e.g. cloud is essential for estimating daily UV doses (e.g. Verdebout (2004)). Comparison of OMI surface UV

150   irradiance estimates with ground-based measurements for Thessaloniki, Greece showed that OMI irradiances overestimate

151   surface observations for UVB wavelengths by between ~1.5% to 13.5% in contrast to underestimated satellite values for UVA

152   wavelengths (Zempila et al., 2016). Results from the validation of TROPOMI surface UV radiation product showed that most

153   of the satellite data agreed within ± 10 % with ground-based measurements for snow-free surfaces (Lakkala et al., 2020).

154   Larger differences between satellite data and ground-based measurements were observed for sites with non-homogeneous

155   topography and non-homogeneous surface albedo conditions. The differences between GB and satellite UVR data are mostly

156   due to uncertainties in the input parameters to the satellite algorithm used to retrieve the UV irradiance at the surface. Based

157   on a recent study of Garane et al. (2019) a mean bias of 0-1.5% and a mean standard deviation of 2.5 – 4.5 % was found for

158   the relative difference between TROPOMI total ozone column (TOC) product and ground based quality assured Brewer and

159   Dobson TOC measurements.

160   In this study we present a UV-Index nowcast and forecast for the European region by using pre-calculated radiative transfer

161   model simulations in the form of analytical look-up tables (LUT) in conjunction with atmospheric input parameters from

162   satellites and high performance computing for instantaneous outputs of the order of 20 million grid points in less than 1 minute.

163   The Earth-Observation-based atmospheric inputs were retrieved operationally for the year 2017 and include the effects of

164   aerosols, clouds, solar and ground elevation, surface albedo and ozone. The aforementioned computing architecture formed a

165   novel system called UVIOS (i.e. UV-Index Operating System). The reliability of the UVIOS input and output parameters was

166   tested against ground-based measurements and an analytical sensitivity analysis was performed in order to quantify the

167   uncertainties and to provide information about the limitations and about the optimum operating conditions of the proposed

168   methodology.

169 In Section 2 we describe the UVIOS, the input data sources and the ground-based measurements used for the validation.

170 Section 3 presents the results in terms of model performance and factors that affect the UVIOS retrievals and the overall

171 accuracy. Finally, Section 4 summarizes the findings and the main conclusions of this study.

172 **2 Data and Methodology**

173 **2.1 The UV Index operating system (UVIOS)**

174 **2.1.1 UVIOS modelling**

175 The UVIOS system is a novel model that uses real-time and forecasted atmospheric inputs based on satellite retrievals and

176 modelling techniques and databases in order to nowcast and forecast the UVI with a spatial resolution of 5 km and a temporal

177 resolution of 15 minutes. The UVIOS calculation scheme is based on the libRadtran library of radiative transfer models (RTM)

178 (Mayer and Kylling, 2005) within which all the available inputs (i.e. solar elevation, cloud and aerosol optical properties,

179 ozone) can be integrated in real-time into the radiative transfer code and calculate the UVI for each pixel. Afterwards, post

180 processing correction for the elevation of each location and the surface albedo is also performed. In order to be able to simulate

181 the UVI for 1.5 million pixels in real-time we use pre-determined spectral solar irradiance LUTs based on the Libradtran RTM,

182 in combination with high performance computing (HPC) architectures that speed up the process of choosing and

183 interpolating/extrapolating the right combinations from the LUTs (Kosmopoulos et al., 2018; Taylor et al., 2016). The result

184 is the retrieval of UVI for 1.5 million pixels covering the European domain in less than 5 minutes after receiving all necessary

185 input parameters.

186 As mentioned the UVIOS architecture does not include a clear sky model and the subsequent calculation of individual sources

187 of UV attenuation, but instead it directly uses the following parameters: solar zenith angle (SZA), the aerosol optical depth

188 (AOD) and other aerosol optical properties (e.g. single scattering albedo (SSA) and Ångström exponent (AE)), the total ozone

189 column (TOC), the cloud optical thickness (COT), as well as the surface elevation (ELE) and the surface albedo (ALB) as

190 RTM inputs. Table 1 presents the EO data used as inputs for the UVI real time simulations, their description and sources. The

191 Meteosat Second Generation (MSG4) cloud microphysics includes the nowcasted cloud optical thickness (COT) at 550 nm,

192 and cloud phase (CPH) obtained at a spatial and temporal resolutions of 5 km (average, depending on latitude) and 15 minutes,

193 respectively. Typical values of other cloud properties (e.g. cloud height, cloud thickness) have been assumed based on the

194 cloud type (information which is also available from MSG) (for more detailed information see Taylor et al. (2016). The 1-day

195 forecast CAMS aerosol optical depth (AOD) at 550 nm is obtained at a spatial and temporal resolutions of 40 km and 3 h,

196 respectively and the monthly aerosol optical properties obtained from Aerocom (Kinne, 2019) includes single scattering albedo

197 (SSA) and Ångström exponent (AE) at 1° x 1° (latitude x longitude) spatial resolution. Solar elevation is taken from the

198 Astronomical model (NREL) (5 km – 15 minutes) and climatological surface albedo (ALB) is retrieved from Copernicus

199 Global Land Service (CGLS) (1 km – 12 days). Surface elevation (ELE) is obtained from the Digital Elevation Model (DEM)

200 of NOAA. The Tropospheric Emission Monitoring Internet Service (TEMIS) 1-day forecast of total ozone column (TOC) is

201 at a spatial resolution of 1º x 1º – 1 day with assimilated ozone fields from GOME-2 (METOP-B). We have to mention also

202 here that the selection of the RTM inputs has been decided based on their real-time availability.

2.1.2 UVIOS real-time processing concept

204 The LUT approach, despite its large size (almost 2.5 million spectral RTM simulations for clear and all sky conditions)

205 (Kosmopoulos et al., 2018), still provides estimates at discrete input parameters values. To overcome this mathematical issue,

206 we performed a multi-parametric interpolation technique to correct the input-output parameter intervals. This solution is

207 computationally more costly than a continuous function-approximation model, i.e. a Neural Network (NN) model

208 (Kosmopoulos et al., 2018), but the accuracy improvement is significant. Indicatively, using a test set of 1 million RTM

209 simulations for UVI from the developed LUT, we applied the NN developed in Kosmopoulos et al. (2018) and found a mean

210 execution time of around 144 seconds followed by a mean absolute error (MAE) of 0.0321, while by using the proposed

211 UVIOS multi-parametric interpolation exploiting the HPC and distributed computing benefits we found for the same test set

212 an execution time of 295 seconds with a MAE of 0.0001. The inclusion of many parameters (in this study we incorporated

213 eight, i.e. AOD, SZA, TOC, COT, ELE, ALB, AE, SSA) with small step sizes dramatically increase the LUT size, followed

214 by high computing requirements for the multi-parametric interpolation/extrapolation procedures.

215 For the UVIOS simulations performed in this study, a 32-core UNIX server was used equipped with 256 Gb of RAM and 12

216 Tb of storage system working in a RAID10 architecture. The combination of the HPC with the analytical LUTs, which were

217 developed by using the libRadtran RTM, allow a high speed multi-parametric interpolation and polynomial reconstruction

218 (Gal, 1986) to increase accuracy between the LUT records following a mathematical equation relating the UVIOS outputs to

219 the EO inputs.

220 An example of the UVIOS input output data is presented in Figure 1 through a flowchart illustration of the modelling technique

221 scheme. The inputs, including the solar and surface elevation, albedo, aerosol, ozone forecasts and the cloud observations as

222 described in Table 1, are fed to the real-time solver that results in spectrally weighted output of UVI for the European region.

223 Figure 2 shows the memory usage and error statistics for a range of different LUT sizes. The LUT error decreases as the LUT

224 size increases, regardless of the function being approximated. The LUT sizes in Figure 2 fit into cache on our HPC

225 environment, thus performance in terms of processing speed and overall output accuracy vary only slightly between the table

226 sizes shown. In our case, UVIOS shows that LUT transformation can provide a significant performance increase without

227 incurring an unreasonable amount of error, provided there is sufficient memory available. We note that the cache size is a

228 critical factor for LUT performance, while under a HPC environment practically there is no limit. Such techniques can be

229 implemented in hardware with distributed computing that operates in parallel to provide optimum performance.

230

2.2 Earth-Observations

231

232 The Cloud Optical Thickness (COT) data from Meteosat was used, whose retrieval algorithm is based on 0.6 and 1.6 micron

233 channel radiances of Meteosat SEVIRI. MSG products have been described in Derrien and Le Gléau (2005) and the

234 MétéoFrance (2013) technical report. The COT impact uncertainty on UVI deals with the MSG COT reliability and accuracy

235 and hence introduces errors into the UVIOS simulations (Derrien and Le Gléau, 2005; Pfeifroth et al., 2016). In addition,

236 comparison principles of (point) station UVI measurements with a 5 km MSG COT matrix are possibly responsible for at least

237 part of the observed deviations (e.g. Kazadzis et al. (2009a)). For instance, when a MSG pixel is partly cloudy, the ground

238 measurements of UVI could fluctuate more than 100%, depending on whether the sun is visible or whether clouds attenuate

239 the direct component of the solar irradiance. The result is that in cases of partly covered MSG pixels and in the absence of

240 clouds between the ground measurement and the sun, the ground truth UVI would be much higher than the UVIOS one. Of

241 course, the presence of small clouds which have not been identified by MSG and cover (part of) the sun disk, is plausible as

242 well, consequently causing an overestimation of the modelled UVI (Koren et al., 2007). Furthermore, sensors onboard

243 geostationary satellites suffer from the parallax error, which contributes to the spatial errors of the images and the overall

244 uncertainty of the products (Bieliński, 2020; Henken et al., 2011). The error depends on the altitude of the cloud and the

245 viewing angle (parallax errors are more significant for high viewing angles).

246 UVIOS calculations at high solar zenith angles (>75 deg) are retrieved assuming cloudless skies since the MSG COT product

247 is not available in these conditions. This has an effect on the quality of the UVIOS overall performance at high solar zenith

248 angles. However, since such measurements are associated with very low UV Index (<1), this inconsistency does not affect

249 UVIOS UV Index results associated with dangerous effects on human health. There is more discussion in the next section on

250 how we use these data for the UVIOS validation.

251 For the total aerosol optical depth, we used 1-day forecast data from the Copernicus Atmospheric Monitoring Service (CAMS)

252 as the basic input parameter. These forecasts are based on the Monitoring Atmospheric Composition and Climate (MACC)

253 analysis and provide accurate data of aerosol optical depth (AOD) at 550 nm with a time step of 1 h and spatial resolution of

254 0.4°.

255 For aerosol single scattering albedo properties climatological values from MACv2 aerosol climatology (Kinne, 2019) was

256 utilized. Monthly means of single scattering albedo at 310nm were acquired from global gridded data at a 1° x 1° spatial

257 resolution. Also, in order to derive the Angstrom exponent, monthly means of AOD at 340nm and 550nm were used. The

258 calculated Ångström exponent was then applied to the 550 nm AOD (from CAMS) in order to get AOD in the UV.

259 The surface albedo data were obtained from the Copernicus global land service (CGLS: Geiger et al., 2008; Carrer et al., 2010).

260 As a global surface ALB product is not available in the UV region, for this study we have used the climatological product of

261 CGLS (in the visible range) as follows: based on the findings of Feister and Grewe, 1995; we used a UV albedo of 0.05 for

262 non-snow cases and a UV ALB equal with CGLS when CGLS exceeded 0.5 (snow cover). The total ozone column forecasts

263 were obtained from Tropospheric Emission Monitoring Internet Service (TEMIS) which is a near- real time service which uses

264 the satellite observations of total ozone column by the Global Ozone Monitoring Experiment (GOME) and SCIAMACHY

265 assimilated in a transport model, driven by the European Centre for Medium-Range Weather Forecasts (ECMWF) forecast

266 meteorological fields (Eskes et al., 2003). The elevation data was obtained from the 5-minute Gridded Global Relief Data

267 (ETOPO5) database, which provides land and seafloor elevation information at a 5-minute latitude/longitude grid, with a 1-

268 meter precision in the region of Europe and is freely available from NOAA (NOAA, 1988). Figure 3 shows an example of the

269 input-output UVIOS parameters. An extensive validation of the MACC analysis and forecasting system products were

270 performed by Eskes et al. (2015). The aerosol optical properties were validated against 3-year (Apr. 2011 – Aug. 2014) near

271 real time level 1.5 Aeronet measurements and for AOD at 550 nm an overall overestimation was exhibited. Due to dedicated

272 validation activity of the MACC service a validation report that covers the time period of this study (Eskes et al., 2018) is also

273 available, presenting an overall positive bias during 2017. This overestimation of AOD at 550 nm may explain some of the

274 UVI underestimation under clear sky conditions (see section 3.2.2).

275 **2.3 Ground-based measurements**

276 In order to validate the UVIOS results 17 ground based stations were selected, for which measurements of the UVI were

277 available during 2017. The stations are shown in Fig. 4. Comparisons were performed with a 15-minute step. The ground based

278 measurements were obtained from spectrophotometers (Brewer), spectroradiometers (Bentham), filter radiometers (GUV) and

279 broadband instruments (SL501 and YES) as Table 2 shows. I Note that UV data in table 2 has been calibrated, processed and

280 provided directly by the responsible scientists for each station. References wherein more information for the data quality of

281 particular instruments can be found are also provided. Brewer spectrophotometers measure the global spectral UV irradiance

282 with a step of 0.5 nm, and a resolution which is approximately 0.5 nm (usually between 0.4 and 0.6 nm). Depending on their

283 type the spectral range is usually 290-325 nm (MKII, MKIV) or 290-363 nm (MKIII,). Since Brewer spectrophotometers

284 measure the spectrum up to a wavelength which is shorter than 400 nm, extension of the spectrum up to 400 nm in order to

285 calculate the UV index is usually achieved using empirical methods (e.g. (Fioletov et al., 2003; Slaper et al., 1995)). The

286 additional uncertainty in the UVI due to the latter approximation is well below the overall uncertainty in the measurements.

287 Bentham spectroradiometers measure the whole UV spectrum (290 – 400 nm) with step and resolution which can be

288 determined by the operator. The spectra from AOS and LIN (measured by Bentham spectroradiometers) used in this study

289 have been recorded with a step of either 0.25 or 0.5 nm and a resolution of ~ 0.5 nm. The Brewer Spectrophotometer measures

290 the total column of ozone using the differential absorption method, i.e. measuring the direct solar irradiance at four wavelengths

291 and then comparing the intensity at wavelengths that are weakly and strongly absorbed by ozone (Kerr et al., 1985). Brewer

292 TOC measurements are used in the present document to validate the TEMIS forecasts. The Ground-based Ultraviolet (GUV)

293 instrument is a multichannel radiometer that measures UV radiation in five spectral bands having central wavelengths as 305,

294 313, 320, 340 and 380 nm. However, in addition to UV irradiances, other data that can be obtained from GUV instruments are

295 total ozone and the cloud optical depth (Dahlback, 1996; Lakkala et al., 2018). GUV measurements are used for LAN station

Atmospheric
Measurement
Techniques
Discussions

296 of Norway. At stations AKR, INN and VIE, the surface UV was measured using Solar Light (SL) 501 radiometers. It provides

297 direct observation of UV index with a frequency of one minute. The Yankee Environmental System (YES) has been used for

298 VAL station. The low latitude stations include AKR, ARE, ATH, ROM, THE, and VAL. AKR has minimum altitude of 23 m

299 and VAL has maximum altitude of 705 m above sea level. The middle latitude locations are AOS, DAV, INN, BEL, LIN,

300 MAN, UCC, and VIE among which the minimum altitude is 10 m in LAN and maximum altitude is in DAV at 1610 m above

301 mean sea level. HEL, LAN, and SOD represent the high latitude zone, with HEL having an altitude of 48 m and SOD an

302 altitude of 185 m above mean sea level (Table 2).

303 A summary of basic climatic information for the validation locations was obtained from the Köppen climate classification

304 (Chen and Chen, 2013) and it is summarized here. THE, AKR, ARE, ROM, ATH and VAL have a Mediterranean climate

305 comprising of mild, wet winters and dry summers. MAN experiences maritime climate (cool summer and cool, but not very

306 cold, winter). AOS, UCC, LAN, BEL, HEL, LIN and VIE experience humid continental climate with warm to hot summers,

307 cold winters and precipitation distributed throughout the year. DAV and INN experience boreal climate characterised by long,

308 usually very cold winters, and short, cool to mild summers. SOD has subarctic climate having very cold winters and mild

309 summers.

310 **2.4 Evaluation methodology**

311 The time series period covers the whole year 2017 at 15-min intervals, following the MSG available time steps. A

312 synchronization between the UVIOS simulations and the ground-based measurements was performed in order to match the

313 15-min intervals of UVIOS to the measured data. The UVIOS data availability is 93%, while for the ground stations it reaches

314 almost 79% enabling a direct UVI data comparison of 77% of the 2017 time steps. For the comparison we used the closest

315 instrument measurements to the 15-min intervals with a maximum deviation of 3 minutes in order to avoid solar elevation and

316 cloud presence mismatches. Additionally, the UVIOS comparisons included measurements up to 70 degrees SZA. The

317 rationale for this cutoff was that UVIOS retrievals at high SZA are retrieved as cloudless as COT is unavailable from MSG.

318 In addition, the comparison is also impacted by limitation of the horizon of ground-based (GB) sites (e.g. Davos, Innsbruck,

319 Aosta) where the diffuse component and in some cases the direct component of solar UV irradiance are affected by obstacles

320 (mountains) on the horizon. The contribution of this mainly diffuse irradiance to the total budget is a function of solar elevation

321 and azimuth (day of the year) and also cloudiness. This explains some of the deviations in the results as the UVIOS retrieves

322 UVI assuming a flat horizon. Clear sky conditions where defined as the UVIOS retrieval where MSG COT equals to zero.

323 Further discussion on the uncertainties introduced by this choice is mentioned in the cloud effect section.

324 Most of the comparisons have been performed using the absolute (mean bias or median) UVI differences (model –

325 measurements). In addition, median values of the percentage differences (100* (model – measurements)/measurements) have

326 been used. UVIOS estimations were also evaluated in terms of mean bias and root mean square error (MBE and RMSE,

327 respectively), defined as follows:

328
$$\mathrm{MBE} = \bar{\varepsilon} = \frac{1}{N}\sum_{i=1}^{N} \varepsilon_i \quad (1) \qquad \mathrm{RMSE} = \sqrt{\frac{1}{N}\sum_{i=1}^{N} \varepsilon_i^2} \quad (2)$$

329   Where $\varepsilon_i = x_f - x_o$ are the residuals (UVIOS errors), calculated as the difference between the simulated values (x_f) and the

330   ground-based values (x_o), and where N is the total number of values. MBE quantifies the overall bias and detects whether the

331   UVIOS overestimates (MBE>0) or underestimates (MBE<0). RMSE quantifies the spread of the error distribution. Finally,

332   the correlation coefficient (r), as well as the coefficient of determination (R^2) were used to represent the proportion of the

333   variability between modeled and measured values.

3 Results

3.1 Performance of the UVIOS technique; result overview

336   Fig. 5 presents a Taylor diagram with the overall UVIOS accuracy for all ground stations under all sky and clear sky conditions

337   as a function of the correlation coefficient, normalized standard deviation and RMSE. Under clear sky conditions, the UVIOS

338   shows the best results with a correlation coefficient (r) close to 0.98 for THE, ROM, AKR, ARE, AOS, and VAL, while the

339   RMSE is below 0.5 UVI for the majority of stations. Under all sky conditions, the error increases with higher uncertainties at

340   MAN, DAV and SOD, which is probably caused by misclassification of cloudy pixels (see also the Appendix A section). For

341   both, clear sky and all sky conditions, the RMSE of the absolute UVI differences between the model and the measurement is

342   close to 0 (within ± 0.5 UVI) for all stations. Most of the comparisons are provided comparing UV Index median values and

343   not percentages. Averaging percentage differences does not provide a fair estimation of the model as such differences in most

344   of the cases are not represented by a normal distribution and also small UVI differences (especially in high cloudiness instants

345   and high solar angles - e.g. differences less than 1 UVI having UVI values less than 1) can differ by up to 500%. Thus, we

346   have focused on absolute differences in order to have a more representative assessment of the actual effect (UV Index) and its

347   results based on low (less than 0.5), moderate (0.5-1) and high (more than 2) UVI differences between UVIOS and the ground

348   based measurements. However, in the Appendix A we also provide such differences in percent.

349   In Table 3, U1.0 and U0.5 represent the percentage of cases with absolute differences between modelled and ground based

350   UVI measurements within 1 and 0.5, respectively, for all comparisons between the 15-minute model retrievals and the

351   corresponding ground-based measurements. As shown in Table 3, for all stations and for both, clear- and all sky conditions,

352   differences were within 0.5 UVI for at least 70% of the cases. Under clear sky conditions, AOS, BEL, HEL, LAN, LIN, SOD

353   and THE had above 90% of U0.5 cases, while others have 75-90% of U0.5 cases. All stations but DAV had above 90% of

354   U1.0 cases for clear skies, while the correlation coefficients for most of the stations were above 0.9 (exceptions are ATH and

355   MAN). For all-skies differences were within 1 UVI for 90% of the cases for all stations with the correlation coefficients

356   exceeding 0.9 for most of them (exceptions are DAV, MAN and SOD). Median differences for all skies for every station were

357   well within ±0.2 UVI, with the 25-75 percentiles being within ±0.5 UVI and the 5-95 percentiles within ±1 UVI. . For clear

Atmospheric
Measurement
Techniques
Discussions

358 skies the corresponding values are ±0.1, ±0.4 and ±0.8 respectively. In the following sections we try to investigate the factors

359 that contribute to the differences between UVIOS and ground-based measurements.

3.2 Factors affecting UVIOS retrievals

3.2.1 Ozone effect

362 All the available collocated Total Ozone Column (TOC) measurements for the stations used in UVIOS evaluation have been

363 obtained from the WOUDC (https://woudc.org/) database. In this database 8 out of 17 UVIOS evaluation stations (AOS, ATH,

364 DAV, MAN, ROM, SOD, THE and UCC) were found, providing TOC GB measurements. TOC comparison has been

365 performed by calculating daily means of GB measurements and the TOC from TEMIS. In order to quantify the effect of the

366 uncertainty of the forecasted TOC used as input at UVIOS we have calculated the mean differences of the forecasted and

367 measured TOCs and used a radiative transfer model to investigate their effect on UVIOS retrieved UVI. Table 4 shows the

368 mean differences in D.U. from TEMIS TOC (used as inputs in UVIOS) as compared to the WOUDC ground-based

369 measurements for one year of comparison data. It is seen that for the stations AOS, DAV, MAN and UCC the values of the

370 TEMIS observations are higher as compared to the ground-based measurements while for the other stations TEMIS

371 observations are lower. The negative bias is seen to be highest for ROM station (-9.9) and the positive bias is highest for AOS

372 station (7.6). Part of the large differences over the complex terrain sites can be explained by the difference between the actual

373 altitude of the station and the average altitude of the corresponding grid points of TEMIS. For example, for AOS the average

374 altitude of the pixel is 2000 m while the real altitude of the station is 570 m, resulting in an underestimation of the tropospheric

375 column of ozone by TEMIS. In general, differences can be explained by the combined effects of uncertainties in TOC retrieval

376 from satellite and GB platforms (Rimmer et al., 2018; Boynard et al., 2018; Garane et al., 2018). Figure 6 shows the effect of

377 this TOC bias on the calculated UVIOS. As seen in Table 4, there is a mix of small underestimation and overestimation cases

378 in the TOCs used within UVIOS, with average absolute differences of 4-5 DU. Worst TOC UVIOS inputs were found in AOS

379 and ROM (7.6 and -9.9 DU) leading to maximum (at 30 degrees SZA) differences in UVI of -0.22 and 0.3 for AOS and ROM,

380 respectively. In general, in most of the cases UVI mean differences are less than 0.1. It has to be noted that the TOC differences

381 have a larger impact when expressed in percent at higher SZAs, while in Figure 6 higher absolute differences for low SZA's

382 are associated with higher UVIs at these SZAs. Detailed comparisons for each station are shown in the Appendix A figures.

3.2.2 Aerosol effect

384 Aerosol optical depth measurements used for the UVIOS aerosol input evaluation have been collected from the AERONET-

385 NASA web site (Giles et al., 2019) for 12 out of our total 17 stations (AKR, ARE, ATH, DAV, HEL, LIN, ROM, SOD, THE,

386 UCC, VAL and VIE. AERONET (level 2, version 3) values of AOD at 500 nm were interpolated at 550nm using the

387 AERONET derived 440-870nm Angstrom exponent for each individual measurement. In order to compare those

388 measurements with CAMS forecasted AOD used for the UVIOS their daily means were derived. The comparison of forecasted
389 and measured daily means was based on all available data due to gaps in the AERONET time series. The AOD MBE and
390 RMSE statistical scores are shown in Table 5 in absolute units and correlation coefficient as well. All the stations have a mean
391 positive bias up to 0.071 except UCC which is showing a mean negative bias of 0.007. The comparison of all individual
392 stations with CAMS data used as inputs on UVIOS showed that under all cases CAMS AOD is higher than that from
393 AERONET with a mean difference of 0.07 at 550nm. The correlation between the modeled and the measured values varies
394 from 0.10 for VIE to 0.91 for ARE with most of the stations showing the correlation coefficient above 0.7. As in the case of
395 the TOC, AOD CAMS data are forecasts from the previous day and real time WOUDC or AERONET level 2.0 data do not
396 exist. Although real time TOC (and in due course AOD in the UV) is available from Eubrewnet (López-Solano et al., 2018;
397 Rimmer et al., 2018), it is only for particular locations and not for the whole European domain. Thus, the only choice in
398 providing for a real time UV Index for Europe is using the CAMS (for AOD) and the TEMIS (for TOC) data.
399 In order to evaluate the effect of AOD on UVI, UVI differences between the UVIOS using both AOD datasets (CAMS and
400 AERONET) as UVIOS inputs were analyzed. Figure 7 shows the mean bias error of the CAMS – AERONET AOD impact on
401 UVI for all stations with available ground based AOD data as a function of SZA together with the uncertainty range ($\pm$ 1 σ).
402 It can be seen that UVIOS with CAMS AOD input underestimates UVI compared to the UVIOS with AERONET data, except
403 for the UCC station. This is consistent with CAMS overestimations of AOD compared to the AERONET measurements,
404 except for the station UCC as shown in Table 5. Higher aerosol levels in the atmosphere tend to lower the UVI. Highest
405 difference in UVI is observed for the stations HEL, SOD, VIE. Since, the aerosol level at the stations HEL and SOD is very
406 low, the percent difference between the AOD from CAMS and AERONET is larger for these stations (although the absolute
407 difference is similar) relative to stations with higher AOD, leading to higher differences in the UVI. Aerosol content for VIE
408 is higher than HEL and SOD but still within 0.2 which might be the reason for the higher UVI difference. In terms of SZA, it
409 is observed that the mean bias decreases with an increase in the SZA as the values of UVI also decrease with SZA and the
410 most deviation is for station VIE which is consistent with the poor correlation between the CAMS forecasted input and the
411 measurements for this station as seen from Table 5.
412 The use of single scattering albedo in the UV region is a difficult task and many studies have shown that such measurements
413 need extra effort and it is not possible to perform them worldwide (Arola et al., 2009; Kazadzis et al., 2016; Raptis et al.,
414 2018). The monthly values of the single scattering albedo used in UVIOS for the UV region were derived from the MACv2
415 database at the 310 nm wavelength (Kinne, 2019). Fig 8 shows the intra annual variability of SSA for the 17 stations. For all
416 stations, SSA values range from 0.76 to 0.93, with most of them having SSA values between 0.83 to 0.93, and relatively small
417 variability. In contrast, there are stations like ARE, BEL, INN, LIN, VIE and THE which have relatively smaller SSA values
418 (0.76-0.9) and greater variability than the other stations.
419
420

3.2.3 Albedo effect

Surface albedo at UV wavelengths is small (2 – 5%) for most types of surfaces (Feister and Grewe, 1995; Madronich, 1993) except for features like sand (with a typical albedo of ~0.3) and snow (up to 1 for fresh snow) (Meinander et al., 2013; Myhre and Myhre, 2003; Vanicek et al., 2000; Henderson-Sellers and Wilson, 1983). Renaud et al. (2000), found an enhancement of about 15 to 25% in UVI for clear-skies and snow conditions due to the multiple ground-atmosphere reflections and this relative increment was about 80% larger for overcast conditions. The combined effect of aerosols and snow lead to an enhancement of about 50% in UVI in cloud-free condition for moderately polluted atmospheres (Badosa and Van Weele, 2002). Fig. 9 presents the effect of surface albedo on the UVI percentage difference (i.e. for various albedo values under clear sky conditions) as a function of SZA. It is observed that the UVI percentage difference increases almost linearly with albedo for a particular SZA and the variation is found to be almost identical for all SZA. This indicates that the UVI percentage difference is independent of the SZA and increases with surface albedo.

Uncertainties introduced in UVIOS from the use of a constant surface albedo value of 0.05 for non-snow conditions are quite low. For the case of albedo values used for snow conditions based on the CGLS monthly mean product uncertainties can be related to: the small difference of UV and visible albedo values; the fact that the CGLS provides an albedo of a certain area around the station that does not necessarily coincide with the "effective" albedo area affecting UV measurements; and finally that the monthly albedo product represents a monthly average while a real time CGLS product represents the last 12 days (dynamically changing albedo). In order to investigate this last point we have compared the UV effects from the use of the two albedo datasets for DAV station. In Fig. 10, the effect of surface albedo correction is shown for the Davos station, for a period with snow cover and low percentage cloudiness. The climatological and the dynamically changing albedo are presented in terms of percentage differences between modelled and ground measurements as a function of SZA. In the case of climatological albedo, most of the percentage difference between forecasted and the measured UVI value is found to vary from -30% to 10% for SZA between 20° to 70°, showing more underestimation than overestimation from the UVIOS simulations. Similarly, in the case of dynamically changing albedo, most of the percentage difference between forecasted and the measured UVI value is found to vary from -20% to 10% for SZA between 20° to 70°. The mean percentage difference between the results using the two different albedo inputs is -2.76% in terms of accuracy improvement. However, beyond 70 degree SZA, there is a huge variation in the percentage difference with mostly underestimations from the UVIOS simulations (not shown in Fig. 10).

3.2.4 Cloud effect

For the evaluation we used measurements at SZA lower than 70 degrees, based on the lack of cloud input from MSG for higher SZAs. The lack of MSG data results in an overestimation of UVIOS in high SZAs and the UVI is systematically overestimated for long periods during winter at high latitude regions when SZA does not get below 70 degrees during the day. However, this overestimation is low in terms of absolute UVI and does not usually exceed 0.2 UVI because maximum UVIs at such SZAs rarely exceed UVI=1.

453 COT retrieved from the MSG satellite has been used as input for the UVIOS together with typical optical properties of the
454 clouds as discussed in Sect. 2.1. The evaluation of all stations for cloudless and cloudy conditions can be seen in Figure 11
455 that shows the relative frequency distribution of all stations (colours) and the mean (black line) for cloudless (upper plot) and
456 cloudy conditions (lower plot). Mean bias error of the modeled by UVIOS and measured UVI for all- and clear sky conditions
457 and the percentage of clear sky time steps data is presented in Figure 12. The mean bias for clear sky conditions is found to be
458 less than that for the all sky condition for the stations AKR, ATH and THE (having most days of the year being cloudless as
459 the clear sky percentage is above 70%). The MBE for DAV, LIN and MAN is less for clear sky relative to all sky conditions
460 even though most days of the year are cloudy (clear sky annual percentage less than 45%) at the particular stations. While,
461 stations BEL, HEL, INN, LAN, SOD, UCC and VIE, that have mostly cloudy skies throughout the year (clear sky annual
462 percentage less than 50%), are having more MBE for clear sky conditions than the all sky condition. This can be due to the
463 erroneous classification of a cloudy sky as clear sky, which is also discussed in the following section. MBE is also larger for
464 AOS and ARE which have mostly clear skies throughout the year. Stations ROM and VAL have comparatively much smaller
465 MBE for clear sky conditions.
466 As shown in Table 6 there are 45.4% of cases with underestimations and 54.6% cases with overestimations for cloudless
467 conditions (COT=0). For all the other cases, overestimations (62.5%) are more predominant than underestimations (37.5%).
468 The difference in the modelled and the measured values goes beyond ± 1 UVI for only 5.1% cases for cloudless condition and
469 14.7% for all other cases. In general, under cloudy conditions, UVIOS shows an overestimation for UVI in contrast to the
470 ground measurements. One explanation for the overestimations could be the erroneous determination of COT from MSG above
471 the ground-based stations, giving cloud input that can be overestimated or underestimated. The results show that there is a
472 general tendency for a small underestimation of MSG COT that leads to a systematic but small UVIOS UVI overestimation
473 under cloudy conditions. Another possible explanation is the spatial representativeness of MSG COT. The MSG COT
474 determination is available at 5 by 5 km pixels that may differ from the actual situation of the cloud prevailing above the station,
475 especially in broken cloud conditions and a case when it blocks the direct radiation from the sun. Moreover, for lower solar
476 elevations, the direct sun irradiance can be blocked by cloud in neighbouring pixels. The first effect has been explored in the
477 relative frequency distribution of Figure 11 that shows a higher number (~ 63%) of data on the right of the zero UVI difference
478 vertical line for cloudy skies. When comparing data outside the 0.5 and 1 difference limits we also see that 1 – 4 times more
479 data show a UVIOS overestimation as compared to the clear sky case. This shows that in general there is a small (in UVI
480 terms) but significant UVIOS overestimation for non-zero COT conditions. Moreover, for clear skies, as determined from the
481 MSG, we observe a less pronounced UVIOS overestimation that corresponds to the fact that even if MSG defines the situation
482 as completely cloudless, in reality there may be some cases where clouds near the GB station affect the measured UVI. This
483 effect is easier to understand when showing these differences as a function of solar zenith angle which is explored through
484 Figure 13. It is observed that the absolute difference between the modelled and the measured values decreases with increasing
485 solar zenith angle and most of the difference lies within ± 4 UVI. The seasonal variation of the percentage UVI difference as

15

486   a function of SZA shows that while absolute UVI is small in winter the percentage difference is higher compared to other

487   seasons.

488   Figure 14 (a) shows the surface horizontal distance as a function of the cloud height and the SZA required for the cloud to

489   block the sun. 14 (b) shows the scatter of the UVI difference under clear sky conditions for all stations as a function of SZA.

490   It is observed that there is an obvious pattern of scattered data for UVI differences higher than 1.5 compared with the ones for

491   differences less than -1.5. These data represent UVIOS overestimation for UVI retrievals due to the underestimation of the

492   cloudiness just above the stations. These data illustrate the well-known spatial representativeness issues whereby a COT value

493   for a satellite grid is not fully representative of a point measurement station. In addition, absolute and percentage relative

494   differences are shown in Fig. 14 (c) and (d) respectively for SZA up to 65 degrees. The differences between the UVIOS and

495   the GB UVI decreases in absolute level but increases in percent with an increase in SZA. This is due to the decrease of UVI

496   with increasing SZA. Modelled and the measured UVI difference is close to zero both for mean and median values. For SZA

497   below 30 degrees differences are 0 to -0.2, while 20 to 80 percentiles range from -0.6 to -0.2. Percentage difference increases

498   with SZA as absolute UVI decreases with the 20 to 80 percentiles showing differences between -10% and 10%

499   **3.2.5 Surface elevation correction**

500   Fig. 15 presents the effect of surface elevation on UVI as a function of the percentage difference for various total ozone

501   columns. The UVI percentage difference is found to increase almost linearly with the increase in elevation for a particular total

502   ozone column. The percentage difference is similar for all ozone columns up to 1km, after which the differences with ozone

503   column become more apparent. That is, at a particular elevation, the percentage difference is higher for less total ozone column.

504   A 1% fluctuation (decline or increase) in column ozone can lead to about a 1.2% fluctuation (increase or decline) in the UV

505   Index (Fioletov et al., 2003; Probst et al., 2012). Indicatively, the surface elevation correction in UVI for the DAV station (due

506   to UVIOS input deviation from to actual elevation) was of the order of 15%, while for INN and AOS it was 6% and for the

507   VAL station close to 8%.

508   **4. Summary and conclusions**

509   In this study, a fast RTM model of UVI, the so-called UVIOS, using inputs of the SZA, aerosol optical depth, total ozone

510   column, cloud optical depth, elevation and surface albedo that implicitly includes temporal effects and the effect of cloud and

511   aerosol physics, allows for the generation of high-resolution maps of UVI. Ground based measurements of UV are the most

512   accurate way to determine this important health related parameter. However, such stations are sparse and hence, satellite

513   observations can be used in order to have a nowcasted UV service. To date polar orbiting satellites like TOMS, OMI and

514   recently TROPOMI provided a global UV dataset with a major disadvantage being the temporal resolution (one measurement

515   per day). This, combined with the large temporal variability of clouds can lead to huge deviations from reality when a single

516   daily measurement is included. Geostationary satellite, MSG, have been used in order to try to improve on such limitations

517   using cloud information every 15 minutes.

518   Comparison of the forecasted and the ground-based measurements indicated that at least 70% and 80% of comparisons were

519   within 0.5 UVI difference for all sky condition and clear sky, respectively. The mean differences TEMIS TOC and the ground

520   measured TOC from the WOUDC for one year of comparison data showed that TEMIS tends to slightly overestimate the TOC

521   for some stations along with underestimating it for other stations. While, in general, in most of the cases UVI mean differences

522   are less than 0.1, the TOC differences have a larger impact in percent UVI differences at higher SZAs. Such small differences

523   can also be the result of daily TOC variation not captured in TEMIS.

524   CAMS AOD seems to be slightly overestimated as compared with AERONET data that leads to a UVIOS underestimation.

525   CAMS data are found to overestimate the AOD from AERONET measurements with a mean difference of 0.07 at 500 nm.

526   All the stations have a mean positive bias up to 0.071 except one station that had a mean negative bias of 0.007. The analysis

527   of the impact of the mean bias error of the CAMS – AERONET AOD impact on UVI for all stations showed that the mean

528   bias decreases with an increase in the SZA as the values of UVI also decreases with SZA. The greatest deviation is for station

529   VIE which is consistent with the poor correlation between the CAMS forecasted input and the measurements for this station.

530   The real time data provision approach of UVIOS requires using a maximum of one-day ozone and aerosol forecast using the

531   TEMIS and CAMS service respectively.

532   Cloudy conditions show high percentage differences but low UVI differences, and have a general tendency to lead to a UVIOS

533   overestimation. It was found that 45.4% of cases have underestimations while 54.6% cases have overestimations for the

534   cloudless conditions, while overestimations (62.5%) were more predominant than underestimations (37.5%) for all the other

535   cases. In general, UVIOS showed an overestimation for UVI in contrast to the ground measurements under cloudy conditions

536   with the difference in the modeled and the measured values going beyond ±1 for 5.1% cases for cloudless conditions and

537   14.7% for all other cases. At individual stations the results for cloudless sky conditions, which are the most important for

538   health related issues, showed good agreement. In general, ~85% of all and 95% of cloudless cases are within 1 UVI difference.

539   The relative percentage biases can be large for low UVI cases due to clouds or at high SZAs, above 75°, due to the absence of

540   accurate information for clouds. The results show that there is a general tendency of small underestimation of MSG COT that

541   leads to a systematic but small UVIOS overestimation under cloudy conditions. Another possible explanation is the spatial

542   representativeness issues between a satellite and a single point on the ground.

543   SSA validation is difficult to perform as there are no systematic SSA measurements in the UV region. Using climatological

544   surface albedo has little impact at low albedo sites but mainly leads to underestimations in UVIOS simulations for high albedo

545   situations (snow cover). Most of the percentage difference between forecasted and the measured UVI values varied from -30%

546   to 10% for SZA between 20° to 70° (climate albedo), while it was found to vary from -20% to 10% for dynamically changing

547   albedo. Since high surface albedo conditions correspond to winter months (i.e. high SZAs and relatively low UVI) for the

548   stations used in the study, the corresponding absolute differences in the UVI are generally smaller than 2 UVI. However, there

549   was a huge variation in the percentage difference beyond 70 degree SZA with mostly underestimations from the UVIOS

550   simulations. Finally, for uncertainties in elevation inputs, the UVI percentage difference is found to increase almost linearly

551   with the increase in elevation for a particular total ozone column and beyond that, it is seen that the rate of increase in the

552   percentage difference decreases with increase in the total ozone column.

553   UVIOS system forms a novel tool for widespread estimations of UVI using real-time and forecasted EO inputs. UVIOS utilizes

554   the MSG domain with high spatiotemporal resolution, producing outputs within acceptable limits of accuracy for UV health

555   related applications. It captures basic cloud features and all major atmospheric and geospatial parameters that affect UVI.

556   Under cloudless conditions it performs to within the uncertainty of the ground based measurements to which it has been

557   compared. Further development and improvement of the model can be achieved in the future. Meteosat Third Generation

558   satellites are expected to be launched in the following years and give aerosol and cloud products which would improve the

559   performance of nowcast and forecast UV models when used as inputs.

560   **Author contribution**

561   PGK was responsible for the design of the study and the whole analysis, with support from SK, AWS, PIR, KP, IF and AM.

562   PGK and SK are the developers of UVIOS. All authors contributed to editing the paper.

563   **Code/Data availability**

564   All data used as inputs to the UVIOS system are open access, while all data sets produced by the UVIOS for the purposes of

565   this paper can be requested from the corresponding author. The ground-based measurements can be requested from the PIs of

566   the stations. The UVIOS suite of algorithms and LUTs can be used for various applications after consultation with the

567   corresponding author.

568   **Competing interests**

569   The authors declare that they have no conflict of interest.

Atmospheric
Measurement
Techniques
Discussions

EGU

576 **References**

577 Arola, A., Kazadzis, S., Lindfors, A., Krotkov, N., Kujanpää, J., Tamminen, J., Bais, A., di Sarra, A., Villaplana, J. M.,
578 Brogniez, C., Siani, A. M., Janouch, M., Weihs, P., Webb, A., Koskela, T., Kouremeti, N., Meloni, D., Buchard, V., Auriol,
579 F., Ialongo, I., Staneck, M., Simic, S., Smedley, A., and Kinne, S.: A new approach to correct for absorbing aerosols in OMI
580 UV, Geophysical Research Letters, 36, 10.1029/2009gl041137, 2009.
581 Badosa, J., and Van Weele, M.: Effects of aerosols on UV-index, KNMI Scientific Report WR-2002-07, 2002.
582 Badosa, J., Calbó, J., McKenzie, R., Liley, B., González, J.-A., Forgan, B., and Long, C. N.: Two Methods for Retrieving UV
583 Index for All Cloud Conditions from Sky Imager Products or Total SW Radiation Measurements, Photochemistry and
584 Photobiology, 90, 941-951, https://doi.org/10.1111/php.12272, 2014.
585 Bais, A. F., Zerefos, C. S., Meleti, C., Ziomas, I. C., and Tourpali, K.: Spectral measurements of solar UVB radiation and its
586 relations to total ozone, SO2, and clouds, Journal of Geophysical Research: Atmospheres, 98, 5199-5204, 10.1029/92jd02904,
587 1993.
588 Bais, A. F., Lucas, R. M., Bornman, J. F., Williamson, C. E., Sulzberger, B., Austin, A. T., Wilson, S. R., Andrady, A. L.,
589 Bernhard, G., McKenzie, R. L., Aucamp, P. J., Madronich, S., Neale, R. E., Yazar, S., Young, A. R., de Gruijl, F. R., Norval,
590 M., Takizawa, Y., Barnes, P. W., Robson, T. M., Robinson, S. A., Ballaré, C. L., Flint, S. D., Neale, P. J., Hylander, S., Rose,
591 K. C., Wängberg, S. Å., Häder, D. P., Worrest, R. C., Zepp, R. G., Paul, N. D., Cory, R. M., Solomon, K. R., Longstreth, J.,
592 Pandey, K. K., Redhwi, H. H., Torikai, A., and Heikkilä, A. M.: Environmental effects of ozone depletion, UV radiation and
593 interactions with climate change: UNEP Environmental Effects Assessment Panel, update 2017, Photochemical &
594 Photobiological Sciences, 17, 127-179, 10.1039/c7pp90043k, 2018.
595 Bais, A. F., Bernhard, G., McKenzie, R. L., Aucamp, P. J., Young, P. J., Ilyas, M., Jöckel, P., and Deushi, M.: Ozone–climate
596 interactions and effects on solar ultraviolet radiation, Photochemical & Photobiological Sciences, 18, 602-640,
597 10.1039/c8pp90059k, 2019.
598 Bernhard, G.: Trends of solar ultraviolet irradiance at Barrow, Alaska, and the effect of measurement uncertainties on trend
599 detection, Atmos. Chem. Phys., 11, 13029-13045, 10.5194/acp-11-13029-2011, 2011.
600 Bernhard, G., and Stierle, S.: Trends of UV Radiation in Antarctica, Atmosphere, 11, 10.3390/atmos11080795, 2020.
601 Bieliński, T.: A Parallax Shift Effect Correction Based on Cloud Height for Geostationary Satellites and Radar Observations,
602 Remote Sensing, 12, 10.3390/rs12030365, 2020.
603 Blumthaler, M., and Ambach, W.: SOLAR UVB-ALBEDO OF VARIOUS SURFACES, Photochemistry and Photobiology,
604 48, 85-88, https://doi.org/10.1111/j.1751-1097.1988.tb02790.x, 1988.
605 Blumthaler, M., Ambach, W., and Ellinger, R.: Increase in solar UV radiation with altitude, Journal of Photochemistry and
606 Photobiology B: Biology, 39, 130-134, https://doi.org/10.1016/S1011-1344(96)00018-8, 1997.
607 Boynard, A., Hurtmans, D., Garane, K., Goutail, F., Hadji-Lazaro, J., Koukouli, M. E., Wespes, C., Vigouroux, C., Keppens,
608 A., Pommereau, J. P., Pazmino, A., Balis, D., Loyola, D., Valks, P., Sussmann, R., Smale, D., Coheur, P. F., and Clerbaux,

609   C.: Validation of the IASI FORLI/EUMETSAT ozone products using satellite (GOME-2), ground-based (Brewer–Dobson,
610   SAOZ, FTIR) and ozonesonde measurements, Atmos. Meas. Tech., 11, 5125-5152, 10.5194/amt-11-5125-2018, 2018.
611   Calbó, J., Pagès, D., and González, J.-A.: Empirical studies of cloud effects on UV radiation: A review, Reviews of
612   Geophysics, 43, 10.1029/2004rg000155, 2005.
613   Carrer, D., Roujean, J.-L., and Meurey, C.: Comparing Operational MSG/SEVIRI Land Surface Albedo Products From Land
614   SAF With Ground Measurements and MODIS, IEEE Transactions on Geoscience and Remote Sensing, 48, 1714-1728,
615   10.1109/TGRS.2009.2034530, 2010.
616   Cede, A., Herman, J., Richter, A., Krotkov, N., and Burrows, J.: Measurements of nitrogen dioxide total column amounts using
617   a Brewer double spectrophotometer in direct Sun mode, Journal of Geophysical Research: Atmospheres, 111,
618   https://doi.org/10.1029/2005JD006585, 2006.
619   Corr, C. A., Krotkov, N., Madronich, S., Slusser, J. R., Holben, B., Gao, W., Flynn, J., Lefer, B., and Kreidenweis, S. M.:
620   Retrieval of aerosol single scattering albedo at ultraviolet wavelengths at the T1 site during MILAGRO, Atmos. Chem. Phys.,
621   9, 5813-5827, 10.5194/acp-9-5813-2009, 2009.
622   Czerwińska, A. E., Krzyścin, J. W., Jarosławski, J., and Posyniak, M.: Effects of urban agglomeration on surface-UV doses: a
623   comparison of Brewer measurements in Warsaw and Belsk, Poland, for the period 2013–2015, Atmos. Chem. Phys., 16,
624   13641-13651, 10.5194/acp-16-13641-2016, 2016.
625   Dahlback, A.: Dahlback, Measurements of biologically effective UV doses, total ozone abundances, and cloud effects with
626   multichannel, moderate bandwidth filter instruments, Appl. Opt. Vol. 35, No. 33, 1996. Further references, see. Eg. Bernhard
627   et al, Johnsen et al. JGR, 2008, Applied Optics, 35, 6514 - 6521, 10.1364/AO.35.006514, 1996.
628   De Bock, V., De Backer, H., Van Malderen, R., Mangold, A., and Delcloo, A.: Relations between erythemal UV dose, global
629   solar radiation, total ozone column and aerosol optical depth at Uccle, Belgium, Atmos. Chem. Phys., 14, 12251-12270,
630   10.5194/acp-14-12251-2014, 2014.
631   Derrien, M., and Le Gléau, H.: MSG/SEVIRI cloud mask and type from SAFNWC, International Journal of Remote Sensing,
632   26, 4707-4732, 10.1080/01431160500166128, 2005.
633   Eleftheratos, K., Kazadzis, S., Zerefos, C. S., Tourpali, K., Meleti, C., Balis, D., Zyrichidou, I., Lakkala, K., Feister, U.,
634   Koskela, T., Heikkilä, A., and Karhu, J. M.: Ozone and Spectroradiometric UV Changes in the Past 20 Years over High
635   Latitudes, Atmosphere-Ocean, 53, 117-125, 10.1080/07055900.2014.919897, 2015.
636   Eskes, H., Huijnen, V., Arola, A., Benedictow, A., Blechschmidt, A. M., Botek, E., Boucher, O., Bouarar, I., Chabrillat, S.,
637   Cuevas, E., Engelen, R., Flentje, H., Gaudel, A., Griesfeller, J., Jones, L., Kapsomenakis, J., Katragkou, E., Kinne, S.,
638   Langerock, B., Razinger, M., Richter, A., Schultz, M., Schulz, M., Sudarchikova, N., Thouret, V., Vrekoussis, M., Wagner,
639   A., and Zerefos, C.: Validation of reactive gases and aerosols in the MACC global analysis and forecast system, Geosci. Model
640   Dev., 8, 3523-3543, 10.5194/gmd-8-3523-2015, 2015.
641   Eskes, H. J., Velthoven, P. F. J. V., Valks, P. J. M., and Kelder, H. M.: Assimilation of GOME total-ozone satellite observations
642   in a three-dimensional tracer-transport model, Quarterly Journal of the Royal Meteorological Society, 129, 1663-1681,
643   https://doi.org/10.1256/qj.02.14, 2003.
644   Eskes, H. J., Wagner, A., Schulz, M., Christophe, Y., Ramonet, M., Basart, S., Benedictow, A., Bennouna, Y., Blechschmidt,
645   A.-M., Chabrillat, S., Clark, H., Cuevas, E., Flentje, H., Hansen, K. M., IM, U., Kapsomenakis, J., Langerock, B., Petersen,
646   K., Richter, A., Sudarchikova, N., Thouret, V., Warneke, T., and Zerefos, C.: Validation report of the cams near-real-time
647   global atmospheric composition service: period September-November 2017., Copernicus Atmosphere Monitoring Service
648   (CAMS) Report, CAMS84_2015SC3_D84.1.1.10_2017SON_V1.pdf, February 2018., 2018.
649   Feister, U., and Grewe, R.: SPECTRAL ALBEDO MEASUREMENTS IN THE UV and VISIBLE REGION OVER
650   DIFFERENT TYPES OF SURFACES, Photochemistry and Photobiology, 62, 736-744, https://doi.org/10.1111/j.1751-
651   1097.1995.tb08723.x, 1995.
652   Fioletov, V., Kerr, J. B., and Fergusson, A.: The UV Index: Definition, Distribution and Factors Affecting It, Canadian Journal
653   of Public Health, 101, I5-I9, 10.1007/bf03405303, 2010.
654   Fioletov, V. E., Kerr, J. B., McArthur, L. J. B., Wardle, D. I., and Mathews, T. W.: Estimating UV Index Climatology over
655   Canada, Journal of Applied Meteorology and Climatology, 42, 417-433, 10.1175/1520-
656   0450(2003)042<0417:EUICOC>2.0.CO;2, 2003.

657   Fioletov, V. E., McArthur, L. J. B., Mathews, T. W., and Marrett, L.: On the relationship between erythemal and vitamin D
658   action spectrum weighted ultraviolet radiation, Journal of Photochemistry and Photobiology B: Biology, 95, 9-16,
659   https://doi.org/10.1016/j.jphotobiol.2008.11.014, 2009.
660   Fountoulakis, I., Bais, A. F., Fragkos, K., Meleti, C., Tourpali, K., and Zempila, M. M.: Short- and long-term variability of
661   spectral solar UV irradiance at Thessaloniki, Greece: effects of changes in aerosols, total ozone and clouds, Atmos. Chem.
662   Phys., 16, 2493-2505, 10.5194/acp-16-2493-2016, 2016.
663   Fountoulakis, I., Zerefos, C. S., Bais, A. F., Kapsomenakis, J., Koukouli, M.-E., Ohkawara, N., Fioletov, V., De Backer, H.,
664   Lakkala, K., Karppinen, T., and Webb, A. R.: Twenty-five years of spectral UV-B measurements over Canada, Europe and
665   Japan: Trends and effects from changes in ozone, aerosols, clouds, and surface reflectivity, Comptes Rendus Geoscience, 350,
666   393-402, https://doi.org/10.1016/j.crte.2018.07.011, 2018.
667   Fountoulakis, I., Natsis, A., Siomos, N., Drosoglou, T., and Bais, F. A.: Deriving Aerosol Absorption Properties from Solar
668   Ultraviolet Radiation Spectral Measurements at Thessaloniki, Greece, Remote Sensing, 11, 10.3390/rs11182179, 2019.
669   Fountoulakis, I., Diémoz, H., Siani, A.-M., Laschewski, G., Filippa, G., Arola, A., Bais, A. F., De Backer, H., Lakkala, K.,
670   Webb, A. R., De Bock, V., Karppinen, T., Garane, K., Kapsomenakis, J., Koukouli, M.-E., and Zerefos, C. S.: Solar UV
671   Irradiance in a Changing Climate: Trends in Europe and the Significance of Spectral Monitoring in Italy, Environments, 7,
672   10.3390/environments7010001, 2020a.
673   Fountoulakis, I., Diémoz, H., Siani, A. M., Hülsen, G., and Gröbner, J.: Monitoring of solar spectral ultraviolet irradiance in
674   Aosta, Italy, Earth Syst. Sci. Data, 12, 2787-2810, 10.5194/essd-12-2787-2020, 2020b.
675   Gal, S.: Computing elementary functions: A new approach for achieving high accuracy and good performance, Accurate
676   Scientific Computations, Berlin, Heidelberg, 1986, 1-16,
677   Garane, K., Bais, A. F., Kazadzis, S., Kazantzidis, A., and Meleti, C.: Monitoring of UV spectral irradiance at Thessaloniki
678   (1990–2005): data re-evaluation and quality control, Ann. Geophys., 24, 3215-3228, 10.5194/angeo-24-3215-2006,
679   2006.
680   Garane, K., Lerot, C., Coldewey-Egbers, M., Verhoelst, T., Koukouli, M. E., Zyrichidou, I., Balis, D. S., Danckaert, T.,
681   Goutail, F., Granville, J., Hubert, D., Keppens, A., Lambert, J. C., Loyola, D., Pommereau, J. P., Van Roozendael, M., and
682   Zehner, C.: Quality assessment of the Ozone_cci Climate Research Data Package (release 2017) – Part 1: Ground-based
683   validation of total ozone column data products, Atmos. Meas. Tech., 11, 1385-1402, 10.5194/amt-11-1385-2018, 2018.
684   Garane, K., Koukouli, M. E., Verhoelst, T., Lerot, C., Heue, K. P., Fioletov, V., Balis, D., Bais, A., Bazureau, A., Dehn, A.,
685   Goutail, F., Granville, J., Griffin, D., Hubert, D., Keppens, A., Lambert, J. C., Loyola, D., McLinden, C., Pazmino, A.,
686   Pommereau, J. P., Redondas, A., Romahn, F., Valks, P., Van Roozendael, M., Xu, J., Zehner, C., Zerefos, C., and Zimmer,
687   W.: TROPOMI/S5P total ozone column data: global ground-based validation and consistency with other satellite missions,
688   Atmos. Meas. Tech., 12, 5263-5287, 10.5194/amt-12-5263-2019, 2019.
689   Giles, D. M., Sinyuk, A., Sorokin, M. G., Schafer, J. S., Smirnov, A., Slutsker, I., Eck, T. F., Holben, B. N., Lewis, J. R.,
690   Campbell, J. R., Welton, E. J., Korkin, S. V., and Lyapustin, A. I.: Advancements in the Aerosol Robotic
691   Network (AERONET) Version 3 database – automated near-real-time quality control algorithm with improved cloud
692   screening for Sun photometer aerosol optical depth (AOD) measurements, Atmos. Meas. Tech., 12, 169-209, 10.5194/amt-12-
693   169-2019, 2019.
694   Gröbner, J., Schreder, J., Kazadzis, S., Bais, A. F., Blumthaler, M., Görts, P., Tax, R., Koskela, T., Seckmeyer, G., Webb, A.
695   R., and Rembges, D.: Traveling reference spectroradiometer for routine quality assurance of spectral solar ultraviolet irradiance
696   measurements, Applied Optics, 44, 5321-5331, 10.1364/ao.44.005321, 2005.
697   Gröbner, J., and Sperfeld, P.: Direct traceability of the portable QASUME irradiance scale to the primary irradiance standard
698   of the PTB, Metrologia, 42, 134-139, 10.1088/0026-1394/42/2/008, 2005.
699   Gröbner, J., Kröger, I., Egli, L., Hülsen, G., Riechelmann, S., and Sperfeld, P.: The high-resolution extraterrestrial solar
700   spectrum (QASUMEFTS) determined from ground-based solar irradiance measurements, Atmos. Meas. Tech., 10, 3375-3383,
701   10.5194/amt-10-3375-2017, 2017.
702   Heikkilä, A., Kaurola, J., Lakkala, K., Karhu, J. M., Kyrö, E., Koskela, T., Engelsen, O., Slaper, H., and Seckmeyer, G.:
703   European UV DataBase (EUVDB) as a repository and quality analyser for solar spectral UV irradiance monitored in
704   Sodankylä, Geosci. Instrum. Method. Data Syst., 5, 333-345, 10.5194/gi-5-333-2016, 2016.
705   Henderson-Sellers, A., and Wilson, M. F.: Surface albedo data for climatic modeling, Reviews of Geophysics, 21, 1743-1778,
706   https://doi.org/10.1029/RG021i008p01743, 1983.

707 Henken, C. C., Schmeits, M. J., Deneke, H., and Roebeling, R. A.: Using MSG-SEVIRI Cloud Physical Properties and Weather
708 Radar Observations for the Detection of Cb/TCu Clouds, Journal of Applied Meteorology and Climatology, 50, 1587-1600,
709 2011.
710 Herman, J. R.: Global increase in UV irradiance during the past 30 years (1979–2008) estimated from satellite data, Journal
711 of Geophysical Research: Atmospheres, 115, 10.1029/2009jd012219, 2010.
712 Holick, M. F.: Vitamin D: the underappreciated D-lightful hormone that is important for skeletal and cellular health, Current
713 Opinion in Endocrinology, Diabetes and Obesity, 9, 2002.
714 Hülsen, G., Gröbner, J., Bais, A., Blumthaler, M., Disterhoft, P., Johnsen, B., Lantz, K. O., Meleti, C., Schreder, J., Vilaplana
715 Guerrero, J. M., and Ylianttila, L.: Intercomparison of erythemal broadband radiometers calibrated by seven UV calibration
716 facilities in Europe and the USA, Atmos. Chem. Phys., 8, 4865-4875, 10.5194/acp-8-4865-2008, 2008.
717 Hülsen, G., Gröbner, J., Nevas, S., Sperfeld, P., Egli, L., Porrovecchio, G., and Smid, M.: Traceability of solar UV
718 measurements using the Qasume reference spectroradiometer, Applied Optics, 55, 7265 - 7275, 10.1364/AO.55.007265, 2016.
719 Hülsen, G., Gröbner, J., Bais, A., Blumthaler, M., Diemoz, H., Bolsee, D., Rodríguez, A. D., Fountoulakis, I., Naranen, E.,
720 Schreder, J., Stefania, F., and Vilaplana Guerrero, J. M.: Second solar ultraviolet radiometer comparison campaign UVC-II,
721 Metrologia, 2020.
722 Juzeniene, A., Brekke, P., Dahlback, A., Andersson-Engels, S., Reichrath, J., Moan, K., Holick, M. F., Grant, W. B., and
723 Moan, J.: Solar radiation and human health, Reports on Progress in Physics, 74, 066701, 10.1088/0034-4885/74/6/066701,
724 2011.
725 Kazadzis, S., Bais, A., Balis, D., Kouremeti, N., Zempila, M., Arola, A., Giannakaki, E., Amiridis, V., and Kazantzidis, A.:
726 Spatial and temporal UV irradiance and aerosol variability within the area of an OMI satellite pixel, Atmos. Chem. Phys., 9,
727 4593-4601, 10.5194/acp-9-4593-2009, 2009a.
728 Kazadzis, S., Kouremeti, N., Bais, A., Kazantzidis, A., and Meleti, C.: Aerosol forcing efficiency in the UVA region from
729 spectral solar irradiance measurements at an urban environment, Ann. Geophys., 27, 2515-2522, 10.5194/angeo-27-2515-
730 2009, 2009b.
731 Kazadzis, S., Raptis, P., Kouremeti, N., Amiridis, V., Arola, A., Gerasopoulos, E., and Schuster, G. L.: Aerosol absorption
732 retrieval at ultraviolet wavelengths in a complex environment, Atmos. Meas. Tech., 9, 5997-6011, 10.5194/amt-9-5997-2016,
733 2016.
734 Kerr, J. B., Evans, W. F. J., and Asbridge, I. A.: Recalibration of Dobson Field Spectrophotometers with a Travelling Brewer
735 Spectrophotometer Standard, Atmospheric Ozone, Dordrecht, 1985, 381-386,
736 Kerr, J. B., and Fioletov, V. E.: Surface ultraviolet radiation, Atmosphere-Ocean, 46, 159-184, 10.3137/ao.460108, 2008.
737 Kinne, S.: The MACv2 aerosol climatology, Tellus B: Chemical and Physical Meteorology, 71, 1-21,
738 10.1080/16000889.2019.1623639, 2019.
739 Koren, I., Remer, L. A., Kaufman, Y. J., Rudich, Y., and Martins, J. V.: On the twilight zone between clouds and aerosols,
740 Geophysical Research Letters, 34, https://doi.org/10.1029/2007GL029253, 2007.
741 Kosmopoulos, P. G., Kazadzis, S., Taylor, M., Raptis, P. I., Keramitsoglou, I., Kiranoudis, C., and Bais, A. F.: Assessment of
742 surface solar irradiance derived from real-time modelling techniques and verification with ground-based measurements,
743 Atmos. Meas. Tech., 11, 907-924, 10.5194/amt-11-907-2018, 2018.
744 Kreuter, A., Buras, R., Mayer, B., Webb, A., Kift, R., Bais, A., Kouremeti, N., and Blumthaler, M.: Solar irradiance in the
745 heterogeneous albedo environment of the Arctic coast: measurements and a 3-D model study, Atmos. Chem. Phys., 14, 5989-
746 6002, 10.5194/acp-14-5989-2014, 2014.
747 Krotkov, N. A., Bhartia, P. K., Herman, J. R., Fioletov, V., and Kerr, J.: Satellite estimation of spectral surface UV irradiance
748 in the presence of tropospheric aerosols: 1. Cloud-free case, Journal of Geophysical Research: Atmospheres, 103, 8779-8793,
749 https://doi.org/10.1029/98JD00233, 1998.
750 Lakkala, K., Arola, A., Heikkilä, A., Kaurola, J., Koskela, T., Kyrö, E., Lindfors, A., Meinander, O., Tanskanen, A., Gröbner,
751 J., and Hülsen, G.: Quality assurance of the Brewer spectral UV measurements in Finland, Atmos. Chem. Phys., 8, 3369-3383,
752 10.5194/acp-8-3369-2008, 2008.
753 Lakkala, K., Redondas, A., Meinander, O., Thölix, L., Hamari, B., Almansa, A. F., Carreno, V., García, R. D., Torres, C.,
754 Deferrari, G., Ochoa, H., Bernhard, G., Sanchez, R., and de Leeuw, G.: UV measurements at Marambio and Ushuaia during
755 2000–2010, Atmos. Chem. Phys., 18, 16019-16031, 10.5194/acp-18-16019-2018, 2018.

Lakkala, K., Kujanpää, J., Brogniez, C., Henriot, N., Arola, A., Aun, M., Auriol, F., Bais, A. F., Bernhard, G., De Bock, V., Catalfamo, M., Deroo, C., Diémoz, H., Egli, L., Forestier, J. B., Fountoulakis, I., Garcia, R. D., Gröbner, J., Hassinen, S., Heikkilä, A., Henderson, S., Hülsen, G., Johnsen, B., Kalakoski, N., Karanikolas, A., Karppinen, T., Lamy, K., León-Luis, S. F., Lindfors, A. V., Metzger, J. M., Minvielle, F., Muskatel, H. B., Portafaix, T., Redondas, A., Sanchez, R., Siani, A. M., Svendby, T., and Tamminen, J.: Validation of TROPOMI Surface UV Radiation Product, Atmos. Meas. Tech. Discuss., 2020, 1-37, 10.5194/amt-2020-121, 2020.

Larkin, A., Haigh, J. D., and Djavidnia, S.: The Effect of Solar UV Irradiance Variations on the Earth's Atmosphere, Space Science Reviews, 94, 199-214, 10.1023/a:1026771307057, 2000.

Levelt, P. F., Oord, G. H. J. v. d., Dobber, M. R., Malkki, A., Huib, V., Johan de, V., Stammes, P., Lundell, J. O. V., and Saari, H.: The ozone monitoring instrument, IEEE Transactions on Geoscience and Remote Sensing, 44, 1093-1101, 10.1109/tgrs.2006.872333, 2006.

Levelt, P. F., Joiner, J., Tamminen, J., Veefkind, J. P., Bhartia, P. K., Stein Zweers, D. C., Duncan, B. N., Streets, D. G., Eskes, H., van der A, R., McLinden, C., Fioletov, V., Carn, S., de Laat, J., DeLand, M., Marchenko, S., McPeters, R., Ziemke, J., Fu, D., Liu, X., Pickering, K., Apituley, A., González Abad, G., Arola, A., Boersma, F., Chan Miller, C., Chance, K., de Graaf, M., Hakkarainen, J., Hassinen, S., Ialongo, I., Kleipool, Q., Krotkov, N., Li, C., Lamsal, L., Newman, P., Nowlan, C., Suleiman, R., Tilstra, L. G., Torres, O., Wang, H., and Wargan, K.: The Ozone Monitoring Instrument: overview of 14 years in space, Atmos. Chem. Phys., 18, 5699-5745, 10.5194/acp-18-5699-2018, 2018.

López-Solano, J., Redondas, A., Carlund, T., Rodriguez-Franco, J. J., Diémoz, H., León-Luis, S. F., Hernández-Cruz, B., Guirado-Fuentes, C., Kouremeti, N., Gröbner, J., Kazadzis, S., Carreño, V., Berjón, A., Santana-Díaz, D., Rodríguez-Valido, M., De Bock, V., Moreta, J. R., Rimmer, J., Smedley, A. R. D., Boulkelia, L., Jepsen, N., Eriksen, P., Bais, A. F., Shirotov, V., Vilaplana, J. M., Wilson, K. M., and Karppinen, T.: Aerosol optical depth in the European Brewer Network, Atmos. Chem. Phys., 18, 3885-3902, 10.5194/acp-18-3885-2018, 2018.

Lucas, R., McMichael, T., Smith, W., Armstrong, B. K., Prüss-Üstün, A., and World Health, O.: Solar ultraviolet radiation : global burden of disease from solar ultraviolet radiation / Robyn Lucas ... [et al.] ; editors, Annette Prüss-Üstün ... [et al.]. Environmental burden of disease series ; no. 13, World Health Organization, Geneva, 2006.

Lucas, R. M., Byrne, S. N., Correale, J., Ilschner, S., and Hart, P. H.: Ultraviolet radiation, vitamin D and multiple sclerosis, Neurodegenerative Disease Management, 5, 413-424, 10.2217/nmt.15.33, 2015.

Madronich, S.: Environmental UV Photobiology, Environ. UV Photobiol., 10.1007/978-1-4899-2406-3, 1993.

Mayer, B., Kylling, A., Madronich, S., and Seckmeyer, G.: Enhanced absorption of UV radiation due to multiple scattering in clouds: Experimental evidence and theoretical explanation, Journal of Geophysical Research: Atmospheres, 103, 31241-31254, https://doi.org/10.1029/98JD02676, 1998.

Mayer, B., and Kylling, A.: Technical note: The libRadtran software package for radiative transfer calculations - description and examples of use, Atmos. Chem. Phys., 5, 1855-1877, 10.5194/acp-5-1855-2005, 2005.

McKenzie, R., Bernhard, G., Liley, B., Disterhoft, P., Rhodes, S., Bais, A., Morgenstern, O., Newman, P., Oman, L., Brogniez, C., and Simic, S.: Success of Montreal Protocol Demonstrated by Comparing High-Quality UV Measurements with "World Avoided" Calculations from Two Chemistry-Climate Models, Scientific Reports, 9, 12332, 10.1038/s41598-019-48625-z, 2019.

McKenzie, R. L., Aucamp, P. J., Bais, A. F., Björn, L. O., Ilyas, M., and Madronich, S.: Ozone depletion and climate change: impacts on UV radiation, Photochemical & Photobiological Sciences, 10, 182-198, 10.1039/c0pp90034f, 2011.

Meinander, O., Kazadzis, S., Arola, A., Riihelä, A., Räisänen, P., Kivi, R., Kontu, A., Kouznetsov, R., Sofiev, M., Svensson, J., Suokanerva, H., Aaltonen, V., Manninen, T., Roujean, J. L., and Hautecoeur, O.: Spectral albedo of seasonal snow during intensive melt period at Sodankylä, beyond the Arctic Circle, Atmos. Chem. Phys., 13, 3793-3810, 10.5194/acp-13-3793-2013, 2013.

MétéoFrance: Algorithm theoretical basis document for cloud products (CMa-PGE01 v3.2, CT-PGE02 v2.2 & CTTH-PGE03 v2.2), Technical Report SAF/NWC/CDOP/MFL/SCI/ATBD/01, Paris: MétéoFrance, 2013.

Mok, J., Krotkov, N. A., Torres, O., Jethva, H., Li, Z., Kim, J., Koo, J. H., Go, S., Irie, H., Labow, G., Eck, T. F., Holben, B. N., Herman, J., Loughman, R. P., Spinei, E., Lee, S. S., Khatri, P., and Campanelli, M.: Comparisons of spectral aerosol single scattering albedo in Seoul, South Korea, Atmos. Meas. Tech., 11, 2295-2311, 10.5194/amt-11-2295-2018, 2018.

Myhre, G., and Myhre, A.: Uncertainties in Radiative Forcing due to Surface Albedo Changes Caused by Land-Use Changes, Journal of Climate, 16, 1511-1524, 10.1175/1520-0442(2003)016<1511:uirfdt>2.0.co;2, 2003.

806 NOAA: Data Announcement 88-MGG-02, Digital relief of the surface of the Earth. NOAA, National Geopgysical Data Center,
807 Boulder, Colorado, 1988.
808 Noël, S., Mieruch, S., Bovensmann, H., and Burrows, J. P.: Preliminary results of GOME-2 water vapour retrievals and first
809 applications in polar regions, Atmos. Chem. Phys., 8, 1519-1529, 10.5194/acp-8-1519-2008, 2008.
810 Peeters, P., Simon, P. C., Hansen, G., Meerkoetter, R., Verdebout, J., Seckmeyer, G., Taalas, P., and Slaper, H.: MAUVE: A
811 European Initiative for Developing and Improving Satellite Derived Ultraviolet Maps, Radiation Protection Dosimetry, 91,
812 201-202, 10.1093/oxfordjournals.rpd.a033200, 2000.
813 Pfeifroth, U., Kothe, S., and Trentmann, J.: Validation report: Meteosat solar surface radiation and effective cloud albedo
814 climate data record (Sarah 2), EUMETSAT SAF CM Validation report with reference number SAF/CM/DWD/VAL/
815 METEOSAT/HEL, 2.1, https://doi.org/10.5676/EUM_SAF_CM/SARAH/V002, 2016.
816 Probst, P., Rizzi, R., Tosi, E., Lucarini, V., and Maestri, T.: Total cloud cover from satellite observations and climate models,
817 Atmospheric Research, 107, 161-170, https://doi.org/10.1016/j.atmosres.2012.01.005, 2012.
818 Raptis, I.-P., Kazadzis, S., Eleftheratos, K., Amiridis, V., and Fountoulakis, I.: Single Scattering Albedo's Spectral Dependence
819 Effect on UV Irradiance., Atmosphere, 9, 10.3390/atmos9090364, 2018.
820 Reda, I., and Andreas, A.: Solar position algorithm for solar radiation applications. NREL Technical Report, NREL/TP-560-
821 34302, Prepared under Task No. WU1D5600, 2008.
822 Renaud, A., Staehelin, J., Fröhlich, C., Philipona, R., and Heimo, A.: Influence of snow and clouds on erythemal UV radiation:
823 Analysis of Swiss measurements and comparison with models, Journal of Geophysical Research: Atmospheres, 105, 4961-
824 4969, https://doi.org/10.1029/1999JD900160, 2000.
825 Rimmer, J. S., Redondas, A., and Karppinen, T.: EuBrewNet – A European Brewer network (COST Action ES1207), an
826 overview, Atmos. Chem. Phys., 18, 10347-10353, 10.5194/acp-18-10347-2018, 2018.
827 Schmalwieser, A., and Siani, A.: Review on Non-Occupational Personal Solar UV Exposure Measurements, Photochemistry
828 and Photobiology, 94, 10.1111/php.12946, 2018.
829 Schmalwieser, A. W., Gröbner, J., Blumthaler, M., Klotz, B., De Backer, H., Bolsée, D., Werner, R., Tomsic, D., Metelka, L.,
830 Eriksen, P., Jepsen, N., Aun, M., Heikkilä, A., Duprat, T., Sandmann, H., Weiss, T., Bais, A., Toth, Z., Siani, A.-M., Vaccaro,
831 L., Diémoz, H., Grifoni, D., Zipoli, G., Lorenzetto, G., Petkov, B. H., di Sarra, A. G., Massen, F., Yousif, C., Aculinin, A. A.,
832 den Outer, P., Svendby, T., Dahlback, A., Johnsen, B., Biszczuk-Jakubowska, J., Krzyscin, J., Henriques, D., Chubarova, N.,
833 Kolarž, P., Mijatovic, Z., Groselj, D., Pribullova, A., Gonzales, J. R. M., Bilbao, J., Guerrero, J. M. V., Serrano, A., Andersson,
834 S., Vuilleumier, L., Webb, A., and O'Hagan, J.: UV Index monitoring in Europe, Photochemical & Photobiological Sciences,
835 16, 1349-1370, 10.1039/c7pp00178a, 2017.
836 Schmalwieser, A. W.: Possibilities to estimate the personal UV radiation exposure from ambient UV radiation measurements,
837 Photochemical & Photobiological Sciences, 19, 1249-1261, 10.1039/d0pp00182a, 2020.
838 Seckmeyer, G., Erb, R., and Albold, A.: Transmittance of a cloud is wavelength-dependent in the UV-range, Geophysical
839 Research Letters, 23, 2753-2755, https://doi.org/10.1029/96GL02614, 1996.
840 Seckmeyer, G., Pissulla, D., Glandorf, M., Henriques, D., Johnsen, B., Webb, A., Siani, A.-M., Bais, A., Kjeldstad, B.,
841 Brogniez, C., Lenoble, J., Gardiner, B., Kirsch, P., Koskela, T., Kaurola, J., Uhlmann, B., Slaper, H., Den Outer, P., Janouch,
842 M., Werle, P., Gröbner, J., Mayer, B., De La Casiniere, A., Simic, S., and Carvalho, F.: Variability of UV Irradiance in Europe,
843 Photochemistry and Photobiology, 84, 172-179, 10.1111/j.1751-1097.2007.00216.x, 2008.
844 Siani, A. M., Casale, G. R., Diémoz, H., Agnesod, G., Kimlin, M. G., Lang, C. A., and Colosimo, A.: Personal UV exposure
845 in high albedo alpine sites, Atmos. Chem. Phys., 8, 3749-3760, 10.5194/acp-8-3749-2008, 2008.
846 Slaper, H., Reinen, H. A. J. M., Blumthaler, M., Huber, M., and Kuik, F.: Comparing ground-level spectrally resolved solar
847 UV measurements using various instruments: A technique resolving effects of wavelength shift and slit width, Geophysical
848 Research Letters, 22, 2721-2724, 10.1029/95gl02824, 1995.
849 Smedley, A. R. D., Rimmer, J. S., Moore, D., Toumi, R., and Webb, A. R.: Total ozone and surface UV trends in the United
850 Kingdom: 1979–2008, International Journal of Climatology, 32, 338-346, 10.1002/joc.2275, 2012.
851 Svendby, T., Hansen, G. H., Bäcklund, A., and Dahlback, A.: Monitoring of the atmospheric ozone layer and natural ultraviolet
852 radiation: Annual report 2018, NILU M-1462 | 2019, 39, 2018.
853 Taylor, M., Kosmopoulos, P. G., Kazadzis, S., Keramitsoglou, I., and Kiranoudis, C. T.: Neural network radiative transfer
854 solvers for the generation of high resolution solar irradiance spectra parameterized by cloud and aerosol parameters, Journal
855 of Quantitative Spectroscopy and Radiative Transfer, 168, 176-192, https://doi.org/10.1016/j.jqsrt.2015.08.018, 2016.

856 Vanicek, K., Frei, T., Litynska, Z., and Schmalwieser, A.: UV-Index for the Public, European Union, 2000.
857 Verdebout, J.: A Satellite-Derived UV Radiation Climatology over Europe to Support Impact Studies, Arctic, Antarctic, and
858 Alpine Research, 36, 357-363, 10.1657/1523-0430(2004)036[0357:asurco]2.0.co;2, 2004.
859 Vitt, R., Laschewski, G., Bais, A. F., Diémoz, H., Fountoulakis, I., Siani, A.-M., and Matzarakis, A.: UV-Index Climatology
860 for Europe Based on Satellite Data, Atmosphere, 11, 10.3390/atmos11070727, 2020.
861 Webb, A. R., and Engelsen, O.: Ultraviolet Exposure Scenarios: Risks of Erythema from Recommendations on Cutaneous
862 Vitamin D Synthesis, in: Sunlight, Vitamin D and Skin Cancer, edited by: Reichrath, J., Springer New York, New York, NY,
863 72-85, 2008.
864 Webb, A. R., Slaper, H., Koepke, P., and Schmalwieser, A. W.: Know Your Standard: Clarifying the CIE Erythema Action
865 Spectrum, Photochemistry and Photobiology, 87, 483-486, 10.1111/j.1751-1097.2010.00871.x, 2011.
866 WHO: Global Solar UV Index: A Pratical Guide, No. WHO/SD., Geneva, Switzerland, 2002.
867 WMO: Report of the WMO Meeting of Experts on UVB Measurements, Data Quality and Standardization of UV Indices,
868 1994, 1995.
869 Zempila, M.-M., Koukouli, M.-E., Bais, A., Fountoulakis, I., Arola, A., Kouremeti, N., and Balis, D.: OMI/Aura UV product
870 validation using NILU-UV ground-based measurements in Thessaloniki, Greece, Atmospheric Environment, 140, 283-297,
871 https://doi.org/10.1016/j.atmosenv.2016.06.009, 2016.
872 Zerefos, C. S., Tourpali, K., Eleftheratos, K., Kazadzis, S., Meleti, C., Feister, U., Koskela, T., and Heikkilä, A.: Evidence of
873 a possible turning point in solar UV-B over Canada, Europe and Japan, Atmos. Chem. Phys., 12, 2469-2477, 10.5194/acp-12-
874 2469-2012, 2012.

875
876
877
878
879
880
881
882
883
884
885
886
887
888
889
890
891
892
893

894

895

896

897

898

899

900

901

Table 1: UVIOS model input parameters

903

Parameter	Description (spatial – temporal resolution)	Source	Reference
Cloud microphysics	Nowcast cloud optical thickness (COT), cloud phase (CPH) (5 km – 15 minutes)	Meteosat Second Generation (MSG4) NOA Antenna	(MétéoFrance, 2013)
Aerosol optical depth	1-day forecast aerosol optical depth (AOD) (40 km – 3 hours)	Copernicus Atmosphere Monitoring Service (CAMS) – FTP access	(Eskes et al., 2015)
Aerosol optical properties	Single scattering albedo (SSA), Angstrom exponent (AE) (1 x 1 degrees – 1 month)	Aerosol Comparisons between Observations and Models (Aerocom)	(Kinne, 2019)
Solar elevation	Solar zenith angle (SZA) (5 km – 15 minutes)	Astronomical model In-house software (NOA)	(Reda and Andreas, 2008))
Surface albedo	Surface albedo (ALB) (1 km – 12 days)	Copernicus Global Land Service (CGLS)	(Carrer et al., 2010)
Water vapor	H_2O observation (40 x 80 km – 1day)	Global Ozone Monitoring Experiment 2 Level 2 data (GOME-2 L2)	(Noël et al., 2008)
Surface elevation	Elevation observation (ELE) (1 m – fixed)	Digital Elevation Model (DEM) In-house database (NOAA)	(NOAA, 1988)
Ozone	1-day forecast total ozone column (TOC) (1 x 1 degrees – 1 day)	Tropospheric Emission Monitoring Internet Service (TEMIS) with Assimilated Ozone Fields from GOME-2 (METOP-B)	(Eskes et al., 2003)

904

905

906

907

908

909

910

911

912

913

914

915

916

917

918

919

920

921

922

923

924
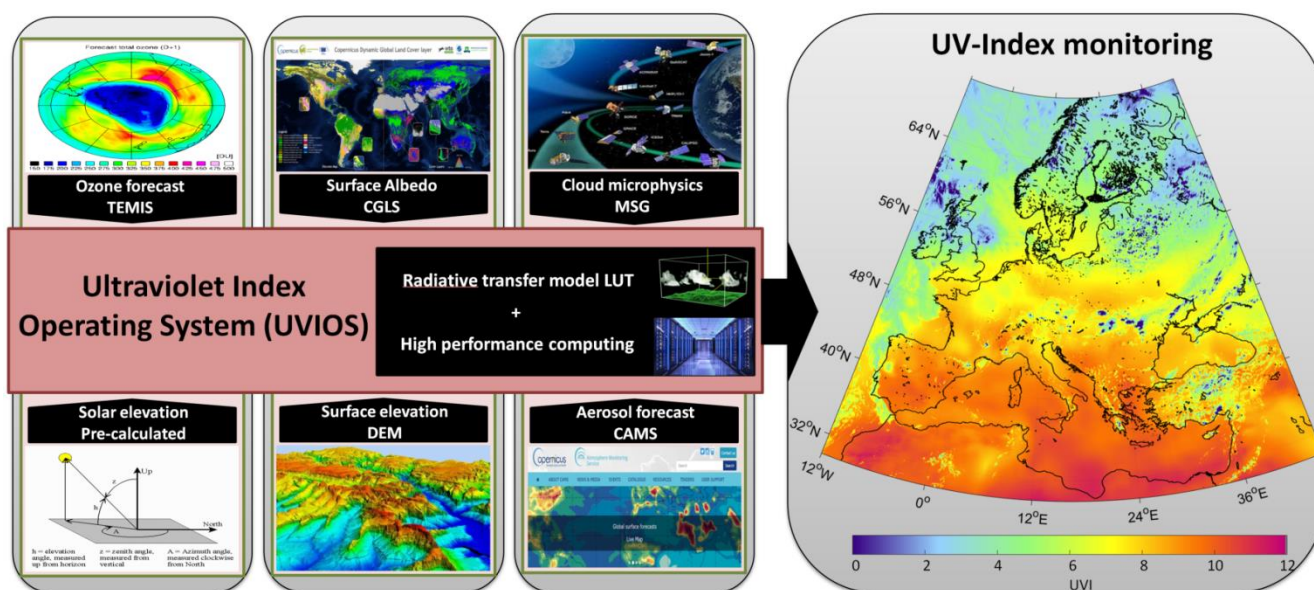
Figure 1: Flowchart illustration of the UVIOS modelling technique scheme. The pre-calculated effects of solar and surface elevation and albedo followed by the aerosol and ozone forecasts and the real-time cloud observations to the UVIOS solver result the spectrally weighted output of UVI for the European region.

928

929

930

931

932

933

934

935

936

937

938

939

940

941

942

Figure 2: UVIOS memory usage and error statistics in terms of mean bias error (MBE) for a range of different LUT sizes.
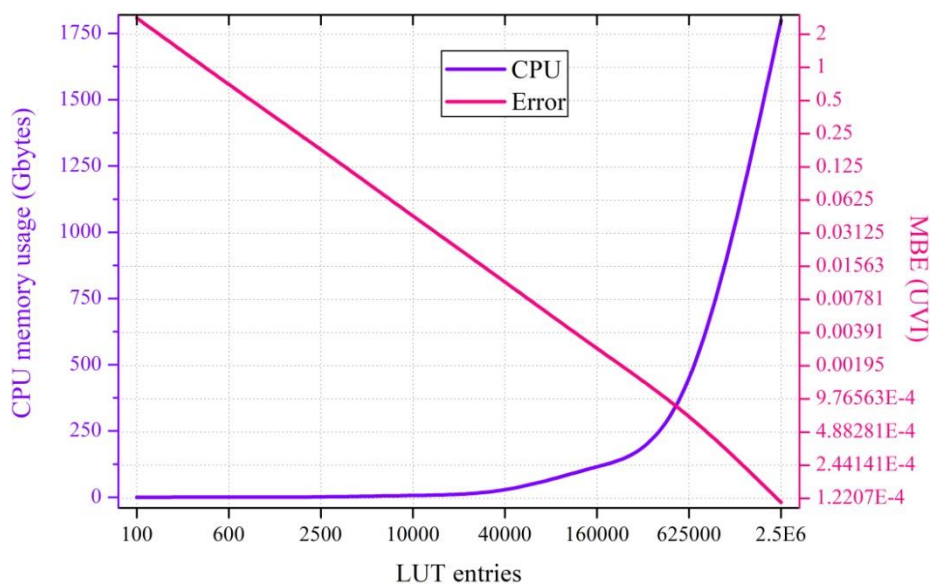
945

946

947

948

949

950

951

952

953
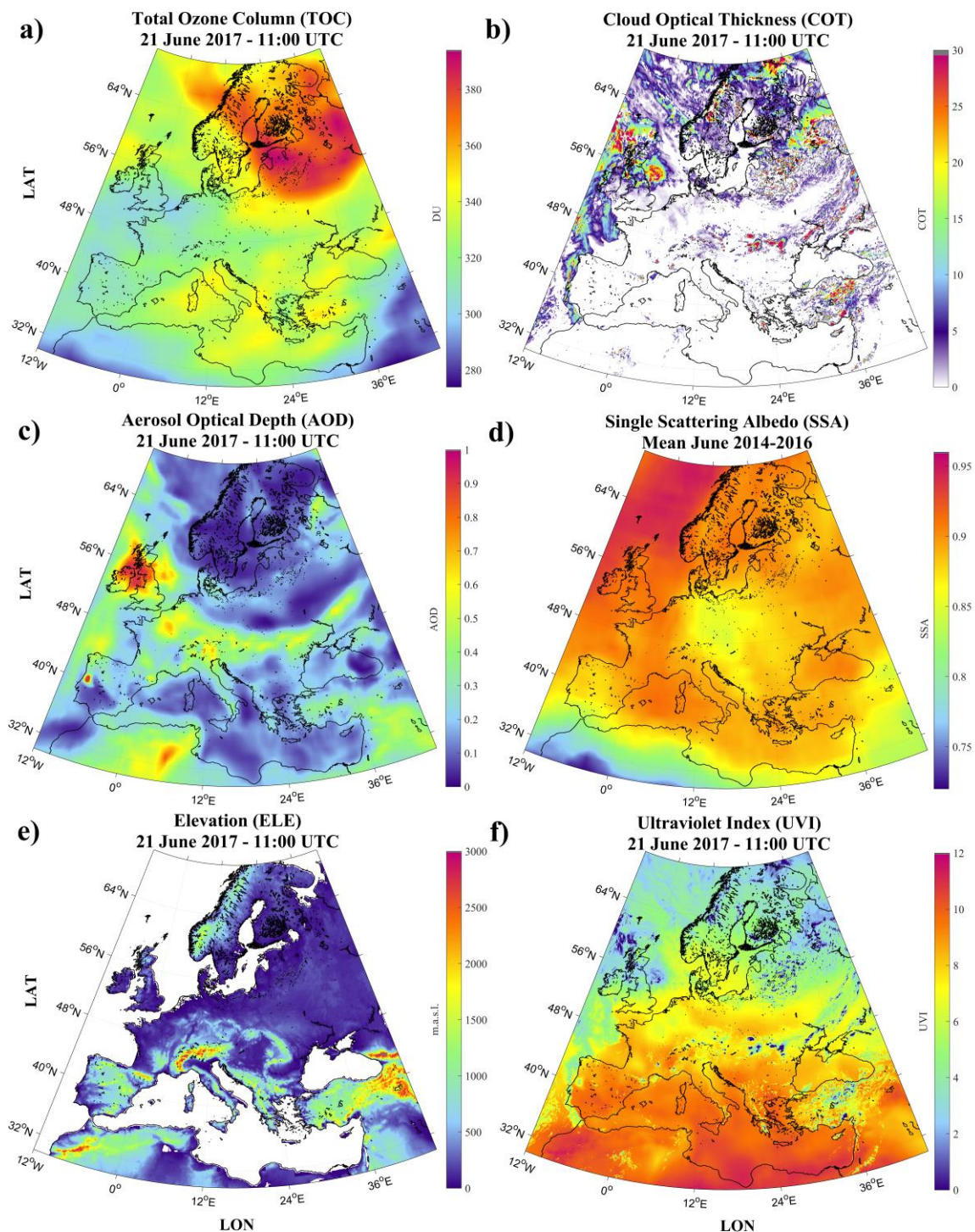
Figure 3: An example of the input TOC (a), COT (b), AOD (c), SSA (d), ELE (e) and output UVI (f) maps based on the UVIOS modelling
technique applied for the 21st of June 2017 at 11:00 UTC.
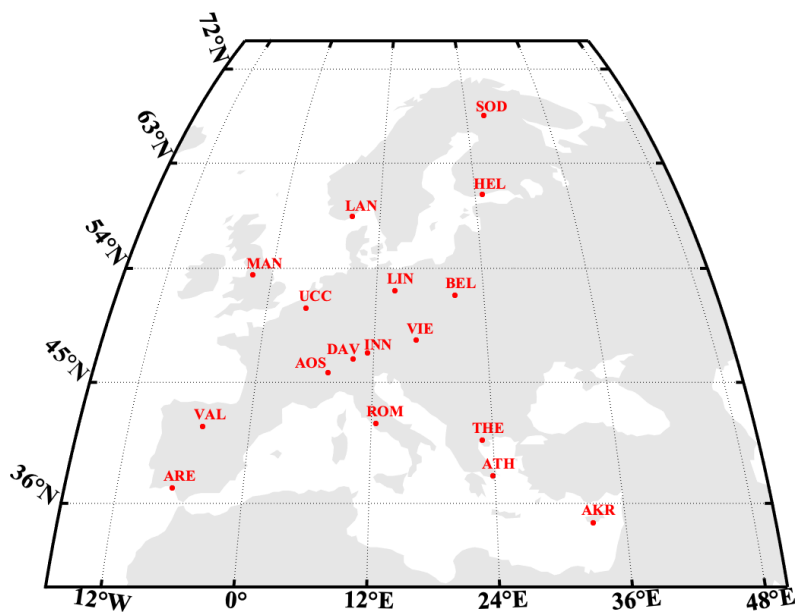
Figure 4: Study region and UVI ground measurement locations.

978

979

980

981

982

983

984 **Table 2:** Coordinates (degrees), instrument type, height (metres above sea level) and maximum UVI measured levels of the European
985 stations used for the comparison.

Station	Country	Code	Latitude (ºN)	Longitude (ºE)	Instrument	Height (m.a.s.l.)	UVImax	Reference
Akrotiri	Cyprus	**AKR**	34.59	32.99	SL501	23	9.14	
Aosta	Italy	**AOS**	45.74	7.36	Bentham DTMc300	570	9.60	(Fountoulakis et al., 2020b)
El Arenosillo	Spain	**ARE**	37.10	-6.73	Brewer MKIII	52	9.78	
Athens	Greece	**ATH**	37.99	23.78	Brewer MKIV	180	10.20	
Belsk	Poland	**BEL**	51.84	20.79	Brewer MKIII	176	7.54	(Czerwińska et al., 2016)
Davos	Switzerland	**DAV**	46.81	9.84	Brewer MKIII	1590	10.57	
Helsinki	Finland	**HEL**	60.20	24.96	Brewer MKIII	48	5.68	(Lakkala et al., 2008)
Innsbruck	Austria	**INN**	47.26	11.38	SL501	577	8.35	(Hülsen et al., 2020)
Landvik	Norway	**LAN**	58.33	8.52	GUV-541	10	6.65	(Svendby et al., 2018)
Lindenberg	Germany	**LIN**	52.21	14.11	Bentham DTMc300	127	8.86	
Manchester	United Kingdom	**MAN**	53.47	-2.23	Brewer MKII	76	7.30	(Smedley et al., 2012)
Rome	Italy	**ROM**	41.90	12.50	Brewer MKIV	75	8.38	
Sodankyla	Finland	**SOD**	67.37	26.63	Brewer MKIII	179	4.51	(Heikkilä et al., 2016; Lakkala et al., 2008)
Thessaloniki	Greece	**THE**	40.63	22.96	Brewer MKIII	60	10.40	(Fountoulakis et al., 2016; Garane et al., 2006)
Uccle	Belgium	**UCC**	50.80	4.35	Brewer MKIII	100	8.99	(De Bock et al., 2014)
Valladolid	Spain	**VAL**	41.66	-4.71	YES	705	10.32	(Hülsen et al., 2020)
Vienna	Austria	**VIE**	48.26	16.43	SL501	153	8.09	(Hülsen et al., 2020)

986

987

988

989

990

991

992

993
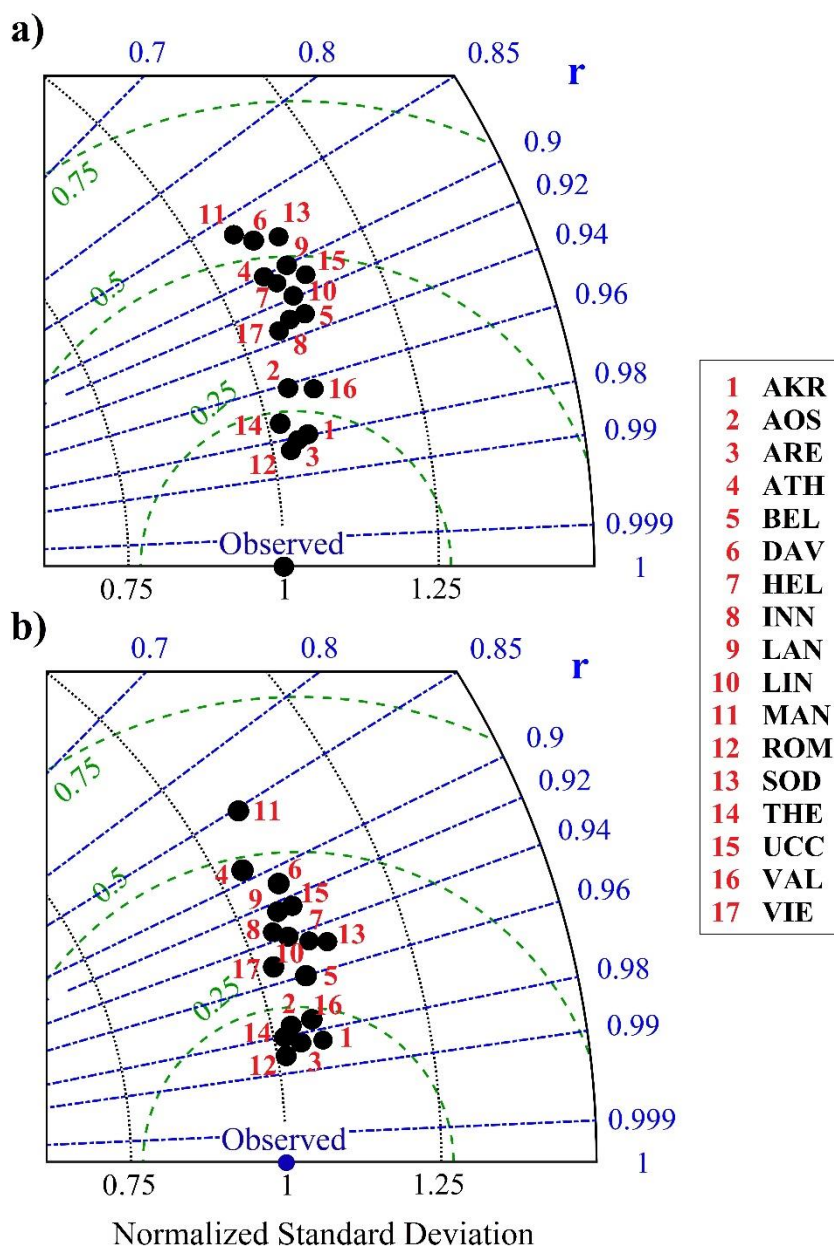
Figure 5: Taylor diagram for the overall UVIOS accuracy for all ground-stations under all sky (a) and clear sky (b) conditions.

997

Atmospheric
Measurement
Techniques

Open Access

EGU

Discussions

998

999

1000

1001

1002

1003

1004

1005

1006

1007

1008 **Table 3:** Absolute difference between modelled and ground based UVI measurements in terms of U0.5 and U1.0 as well as the R for all sky
1009 and clear sky conditions.

STATION	ALL SKY			CLEAR SKY		
	U0.5	U1.0	R	U0.5	U1.0	R
AKR	82.25	96.02	0.980	84.57	97.48	0.987
AOS	86.81	94.40	0.961	92.23	97.07	0.978
ARE	85.15	95.73	0.981	87.99	96.86	0.986
ATH	84.99	94.29	0.902	88.98	96.35	0.891
BEL	83.07	93.28	0.933	91.30	96.50	0.960
DAV	74.20	86.43	0.873	76.19	87.06	0.912
HEL	86.53	94.79	0.909	94.13	97.70	0.944
INN	79.96	92.17	0.932	87.09	95.23	0.937
LAN	84.94	93.46	0.900	92.34	96.52	0.925
LIN	81.58	91.86	0.919	90.95	96.31	0.941
MAN	77.72	90.44	0.862	87.85	94.27	0.852
ROM	87.69	96.19	0.985	89.55	97.00	0.991
SOD	90.86	97.26	0.883	95.69	98.94	0.947
THE	88.98	95.91	0.974	92.51	97.35	0.981
UCC	71.18	87.68	0.913	83.23	92.15	0.926
VAL	85.86	93.93	0.962	86.61	95.22	0.976
VIE	76.65	91.53	0.936	83.37	94.42	0.952

1010

1011

1012

1013

1014

1015

1016

1017

1018

1019

1020

1021

1022

1023

1024

1025

1026

1027

1028

1029

1030

1031

1032

1033

1034

1035

1036

Table 4: Mean bias error of the TEMIS TOC as compared to the WOUDC ground-based measurements.

Station	AOS	ATH	DAV	MAN	ROM	SOD	THE	UCC
MBE TOC (DU)	7.6	-0.9	1.9	5.0	-9.9	-5.4	-2.2	2.9

1037

1038

1039

1040

1041

1042

1043

1044

1045

1046

1047

1048

1049

1050

1051

1052

1053

1054

1055

1056

1057

1058

1059

1060

1061

1062

1063

Figure 6: Differences of UVI derived by the UVIOS using as input the TEMIS and the Brewer TOC respectively at all stations with available data. (lower possible SOD SZA is 44 degrees).
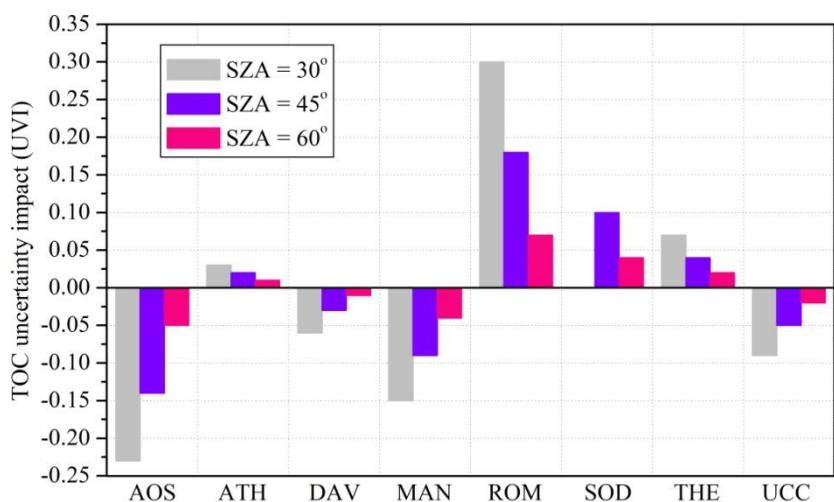
1066

1067

1068

1069

1070

1071

1072

1073

1074

1075

1076

1077

1078

1079

1080

1081

1082

1083

1084

1085

1086

1087

1088

Table 5: Comparison results between CAMS forecasted AOD values used as UVIOS input and AERONET ground-based AOD measurements. The AOD MBE and RMSE statistical scores are shown in absolute units, along with correlation coefficient.

Station	AKR	ARE	ATH	DAV	HEL	LIN	ROM	SOD	THE	UCC	VAL	VIE
MBE	0.037	0.042	0.030	0.029	0.062	0.026	0.017	0.047	0.008	-0.007	0.024	0.071
RMSE	0.074	0.070	0.074	0.053	0.078	0.074	0.056	0.065	0.066	0.150	0.073	0.157
R	0.77	0.91	0.80	0.73	0.70	0.69	0.80	0.63	0.76	0.50	0.78	0.10

1091
1092

1093

1094

1095

1096

1097

1098

1099

1100

1101

1102

1103

1104

Atmospheric
Measurement
Techniques
Discussions

Open Access
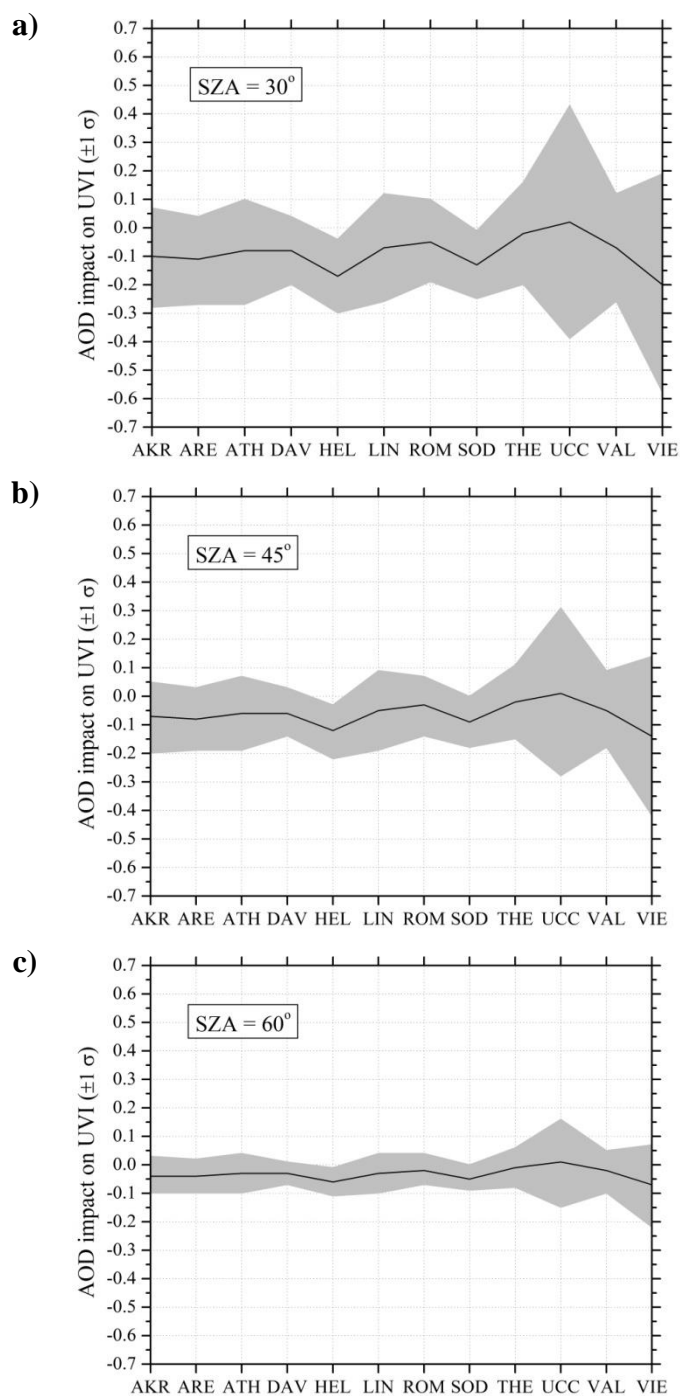
Figure 7: The mean bias error of the CAMS – AERONET AOD impact on UVI for all stations with available data as a function of SZA at 30 (a), 45 (b) and 60 (c) degrees together with the uncertainty range (± 1 σ).

1108

1109

1110

1111

1112

1113

1114

Figure 8: The monthly mean (i.e. 1-12 = Jan-Dec) SSA levels for all ground stations as derived by the MACv2 database.
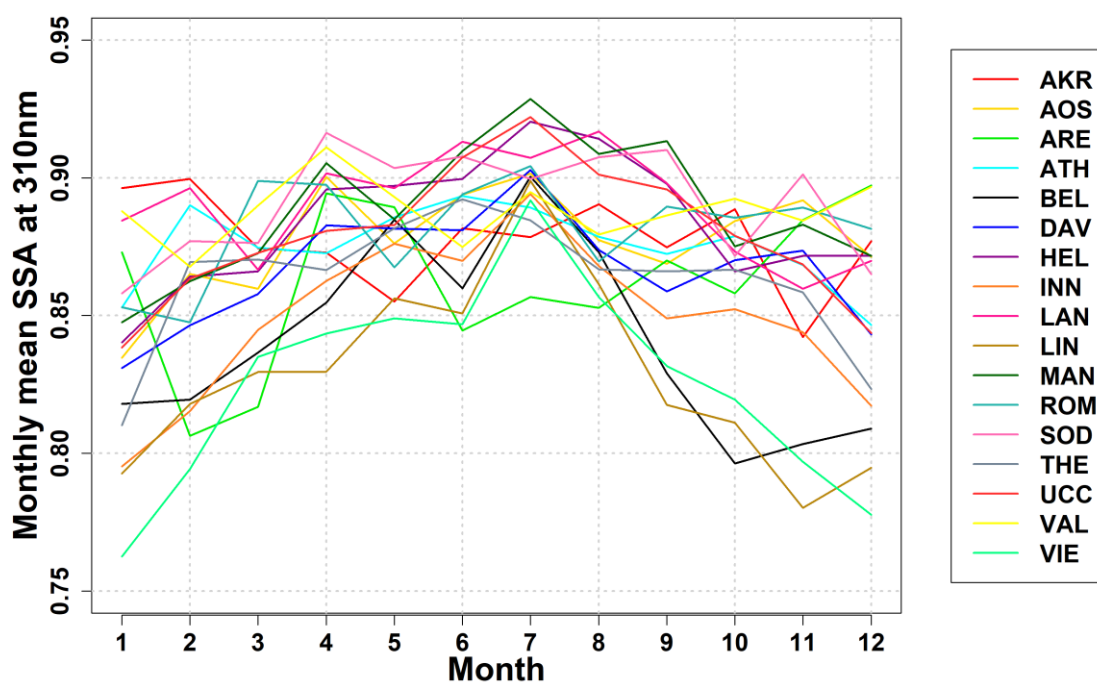
1117

1118

1119

1120

1121

1122

1123

1124

1125

1126

1127

1128

1129

1130

1131

1132

1133

1134

1135

1136

Figure 9: The surface albedo effect on UVI as a function of percentage difference for various SZAs.
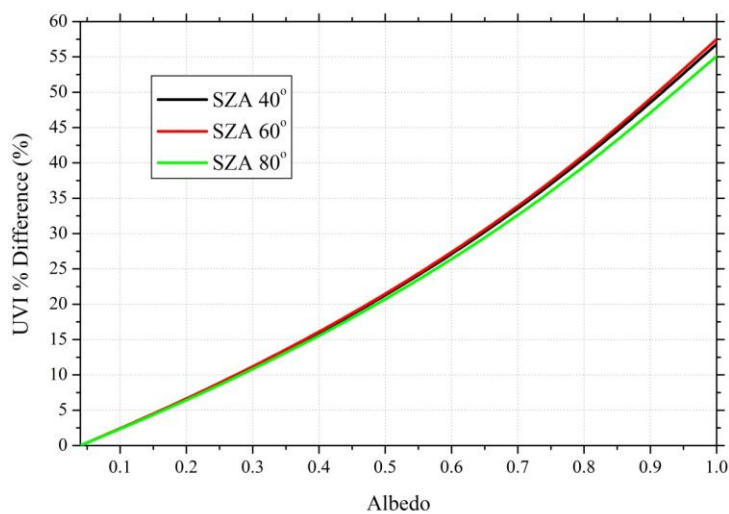
1138

1139

1140

1141

1142

1143

1144

1145

1146

1147

1148

1149

1150

1151

1152

1153

1154

1155

1156

1157

1158
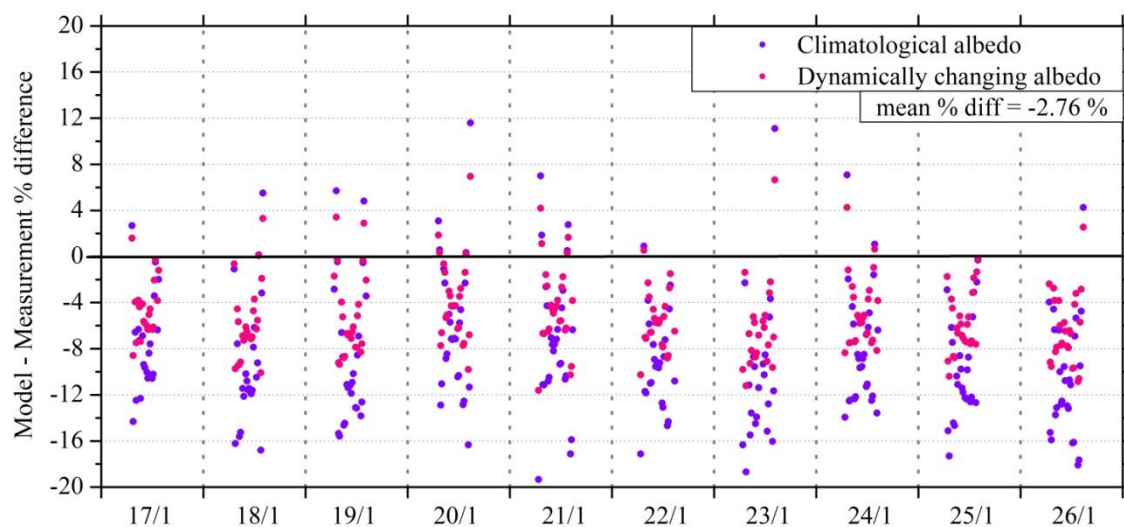
Figure 10: The effect of surface albedo correction on UVI for the Davos station. The climatological and the dynamically changing albedo in terms of percentage differences of modelled and ground measurements during a snow covered period (17/1 - 26/1) under clear sky conditions.

1159

1160
1161
1162

1163

1164

1165

1166

1167

1168

1169

1170

1171
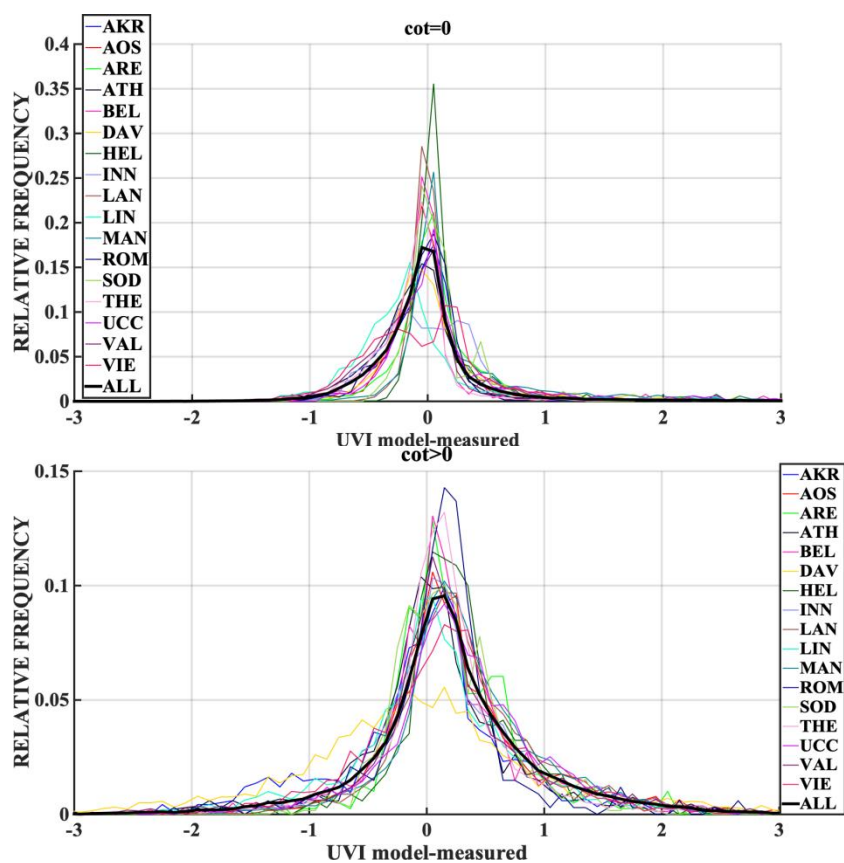
Figure 11: Relative frequency distribution of UVI residuals for all stations (coloured lines) and the mean (black line) for cloudless (upper plot) and cloudy (lower plot) conditions.
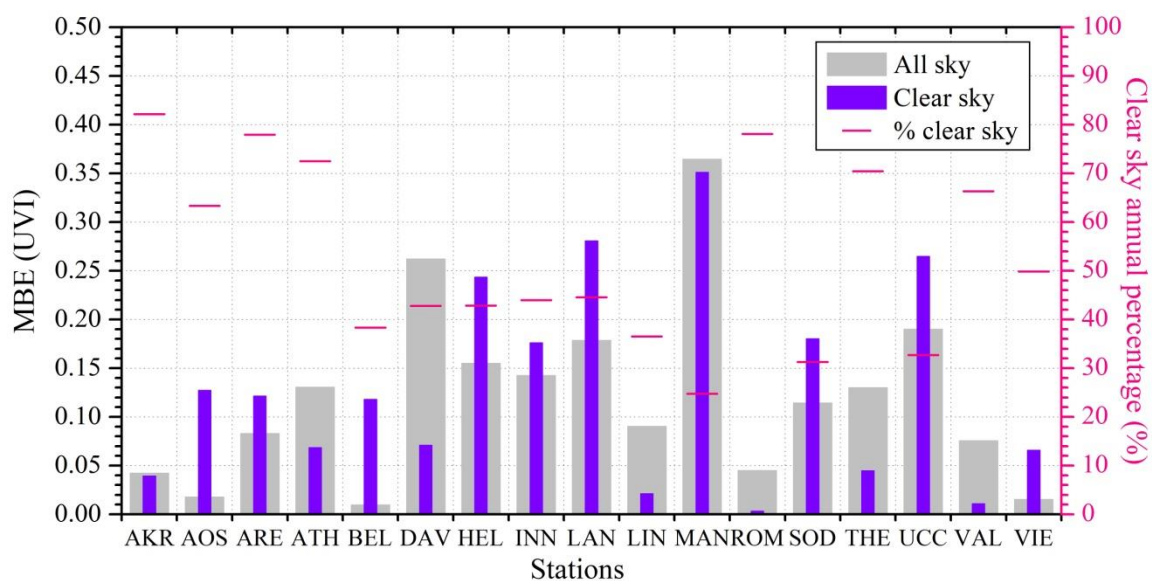
Figure 12: Mean bias error of the modelled UVI as compared to the ground-based measurements for all and clear sky conditions. The percentage of clear sky data time steps was also plotted with red lines.

Atmospheric
Measurement
Techniques
Discussions

1210

1211

1212

1213

1214

1215

1216

1217

1218

1219

1220

1221

1222

1223

1224

1225 **Table 6:** Percentage of data for UVIOS underestimation (A1-A3) and overestimation (B1-B3) under clear and cloudy sky conditions for

1226 various UVI difference (modelled-ground) classes.

Difference of UVI	< -1.0 (A1)	< -0.5 (A2)	< 0.0 (A3)	> 0.0 (B3)	> 0.5 (B2)	> 1.0 (B1)
% of data COT > 0	3.6	11.5	37.5	62.5	24.8	11.1
% of data COT = 0	0.9	10.2	45.4	54.6	11.4	4.2

1227

1228

1229

1230

1231

1232

1233

1234

1235

1236

1237

1238

1239

1240

1241

1242

1243

1244

1245

1246

1247

1248

1249

1250

1251

1252

1253
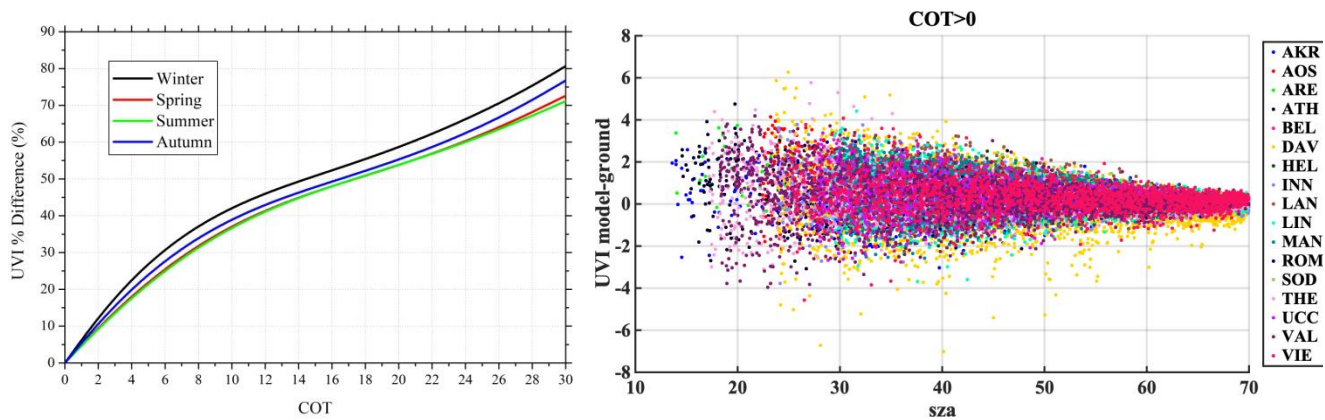
Figure 13: The average COT effect on UVI as a function of percentage difference for all seasons (left) and scatterplot of the UVI difference under cloudy sky conditions for all stations (right).

1256

1257

1258

1259

1260

1261

1262

1263

1264

1265

1266

1267

1268

1269

1270

1271

1272
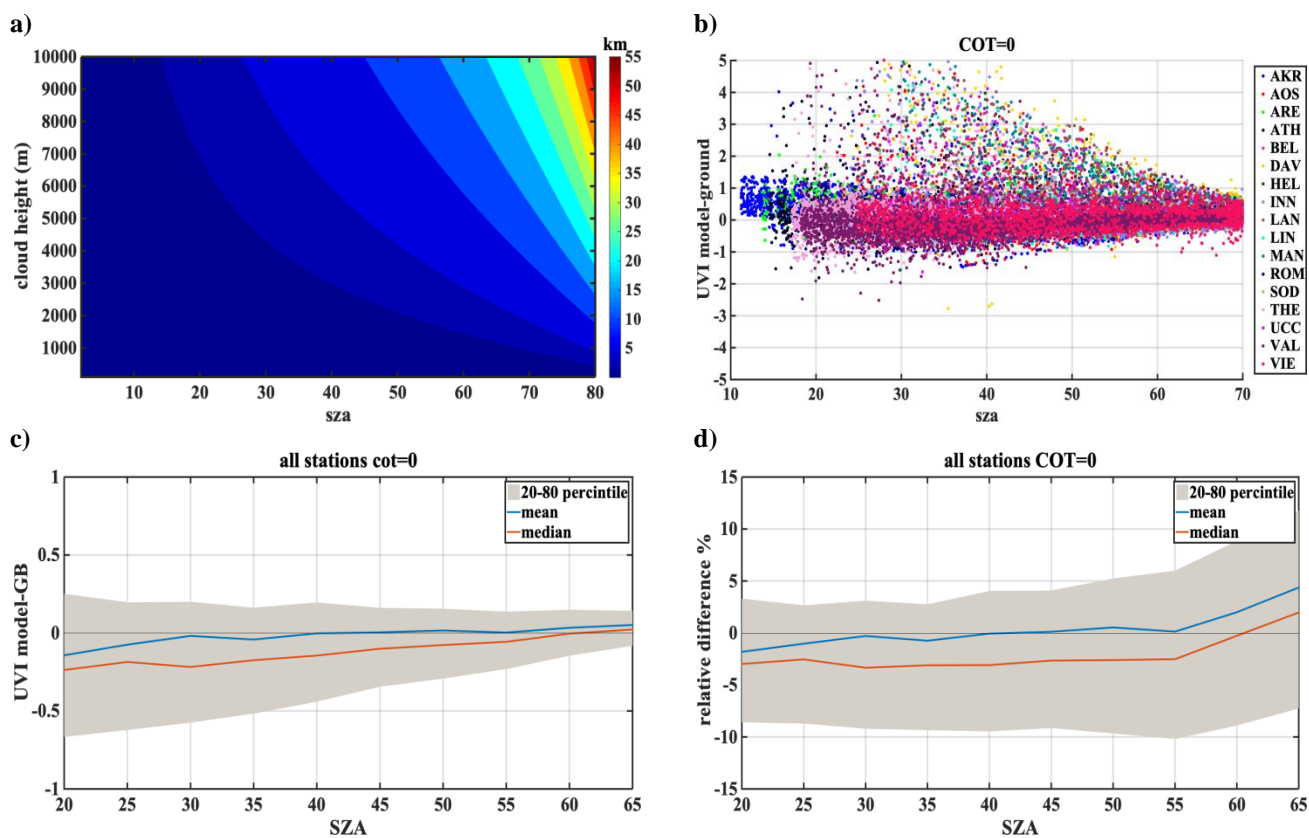
1273

Figure 14: a). The surface distance of the projection of a cloud relative to the instrument in order to block the sun as a function of the cloud height and the SZA . (b). Scatterplot of the UVI difference under clear sky conditions for all stations. c-d) UVI mean, median and 20-80 percentile differences (c) and percentage differences (d) derived by the UVIOS as compared to the ground-based measurements for clear sky conditions as a function of SZA.

1278

1279

1280

1281

1282

1283

1284

1285

1286

1287

1288

1289

1290

1291

1292

Figure 15: The surface elevation effect on UVI as a function of percentage difference for various total ozone columns.
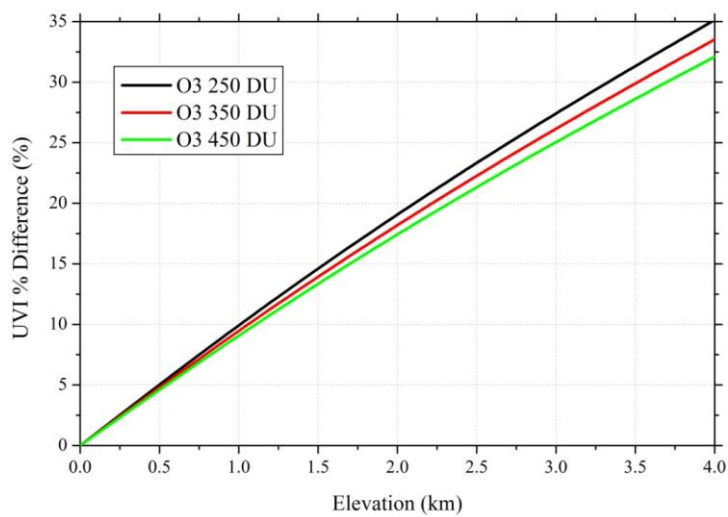
1295

1296

1297

1298

1299

1300

1301

1302

1303

Appendix A

The following set of Figures (A.1 – A.17) show for all stations, density scatterplots of measured and modeled UVI for all sky and clear sky conditions (upper row), normalized probability histogram of differences (middle row), and boxplot of differences (lower row) as a function of SZA, representing median (red lines), mean (blue dotted lines) 25-75 percentiles (blue boxes) and 5-95 whiskers (dotted lines).Table A.1 shows additionally the amount of data points that represent both all sky and clear sky conditions for the studied stations.

We have categorized the stations mostly based on cloud cover as Mediterranean, Central Europe, High altitude and High latitude. Each of the station has its own characteristics in terms of atmospheric conditions and parameters affecting the UVI reaching the ground. A summary of the results with possible explanation of the differences observed are shown here. The Mediterranean region includes the stations THE, ATH, AKR, ROM, VAL and ARE. Analysis of TOC showed that in most of the cases UVI mean differences are less than 0.1 in general while a negative bias between TOC and the ground measurements was seen to be highest for ROM (-9.9) that corresponds to the UVI difference of 0.3. Impact of AOD uncertainty showed the correlation coefficient between the modelled and the measured UVI values above 0.7 for most of the stations while it was as high as 0.91 for ARE. The mean bias between the modelled and measured UVI for clear sky condition was found to be less than that for the all sky condition for the stations AKR, ATH and THE that had most days of the year as cloud-free (the clear sky percentage is above 70%). The mean bias between the modelled and measured UVI for clear sky condition was more than the all sky condition for ARE even though it had mostly clear skies throughout the year. The analysis of the combined effect of the aerosol and ozone at Thessaloniki revealed that the model showed a slight underestimation with real inputs (AERONET and Brewer) while overestimations for forecasted inputs (CAMS and TEMIS). However, the coefficient of correlation was found to be as 0.989 and 0.992 for the model with forecasted and real inputs, respectively. Stations of this classification have the single scattering albedo ranging from 0.76 to 0.93, with most of them having SSA values between 0.83 to 0.93 except stations ARE and THE that had relatively smaller SSA values (0.76-0.9) and greater variability, and large MBE. AKR station comparison showed some UVIOS calculated UVI at higher levels than the GB measurements especially in low SZA's. However, GB UVI measurements seem more unrealistic than the UVIOS calculated UVI for summer local noon conditions as modeled UVIs with real AOD and TOC measurements at the area tend to agree with UVIOS outputs.

The second classification is the Central European regions including AOS, UCC, BEL, MAN, LIN, VIE and INN. The median of the absolute UVI differences between the model and the measurement for all sky condition were higher for MAN and UCC while for others it was close to zero. Larger UVI difference of -0.22 due to TOC uncertainty impact was observed for AOS which might be due to large values of UVI at higher altitude as the positive bias is highest for AOS station (7.6). The UVIOS MBE and RMSE statistical scores for analyzing AOD uncertainty impact showed a mean positive bias up to 0.071 for all the stations except UCC which is showed a mean negative bias of 0.007. The mean bias between the modelled and measured UVI for clear sky condition was more than the all sky condition for AOS even though it had mostly clear skies throughout the year. BEL, UCC and VIE showed more MBE for clear sky condition than the all sky condition as they have mostly cloudy skies

47

Atmospheric
Measurement
Techniques
Discussions

1337 throughout the year (clear sky annual percentage less than 50%). However, stations LIN and MAN also have more MBE for

1338 clear sky condition even though they have most days of the year as cloudy (clear sky annual percentage less than 45%).

1339 Analysis of AOD uncertainty showed that UVI difference was highest for VIE than the other stations. The monthly values of

1340 the single scattering albedo used in UVIOS ranged from 0.76 to 0.93 for stations AOS, UCC and MAN, with most of them

1341 having SSA values between 0.83 to 0.93, and relatively small variability. While, the stations BEL, INN, LIN and VIE had

1342 relatively smaller SSA values (0.76-0.9) and greater variability than the other stations and most of these stations have shown

1343 large MBE.

1344 The high altitude station is DAV and high latitude stations include LAN, HEL and SOD. DAV have less MBE for clear sky

1345 condition even though they have most days of the year as cloudy (clear sky annual percentage less than 45%). DAV and MAN

1346 show worse statistical behavior for clear sky, which is probably caused by misclassification of cloudy pixels. For DAV this

1347 could be explained by the complex mountainous topography of the area. Large UVI differences in SOD and HEL indicate

1348 higher introduced uncertainties over higher latitudes. Higher aerosol levels in the atmosphere tend to lower the UVI. Highest

1349 difference in UVI is observed for the stations HEL, SOD and VIE. Since, the aerosol level at the stations HEL and SOD is

1350 very low this leads to higher UVI which can be the reason for th small UVI differences observed for these stations. Stations of

1351 this classification have mostly cloudy skies throughout the year (clear sky annual percentage less than 50%) and have more

1352 MBE for clear sky condition than the all sky condition. This might be due the fact that the clouds are not captured well at a

1353 point station and a cloudy sky might have been considered as a clear sky. Higher UVI difference was observed for HEL and

1354 SOD as a result of AOD uncertainty analysis which might be due to the low aerosol content of these stations due to higher

1355 latitude that leads to higher UVI values.

1356

1357 Table A.1 Number of data points and clear sky data points, used in the analysis for each station.

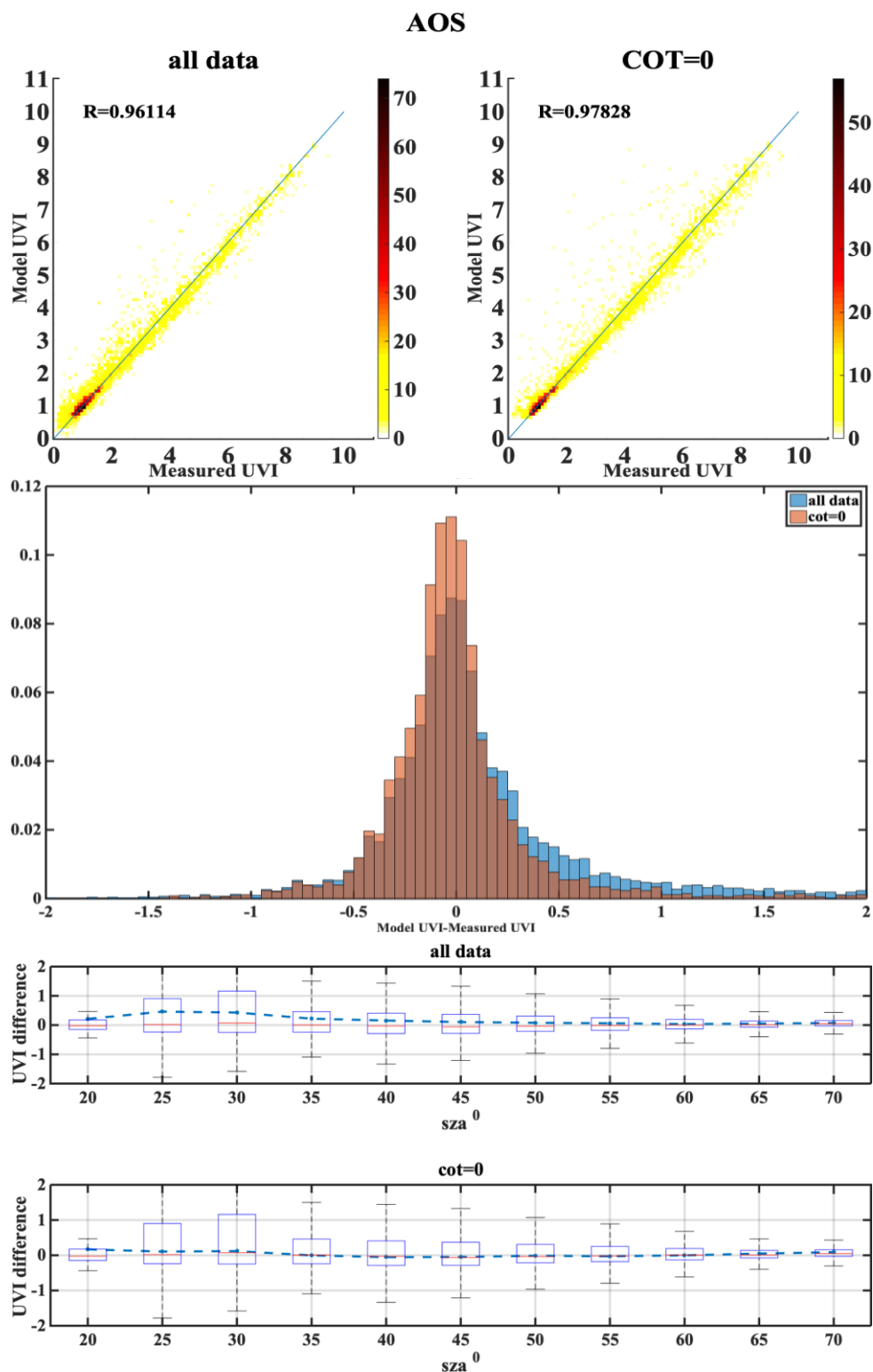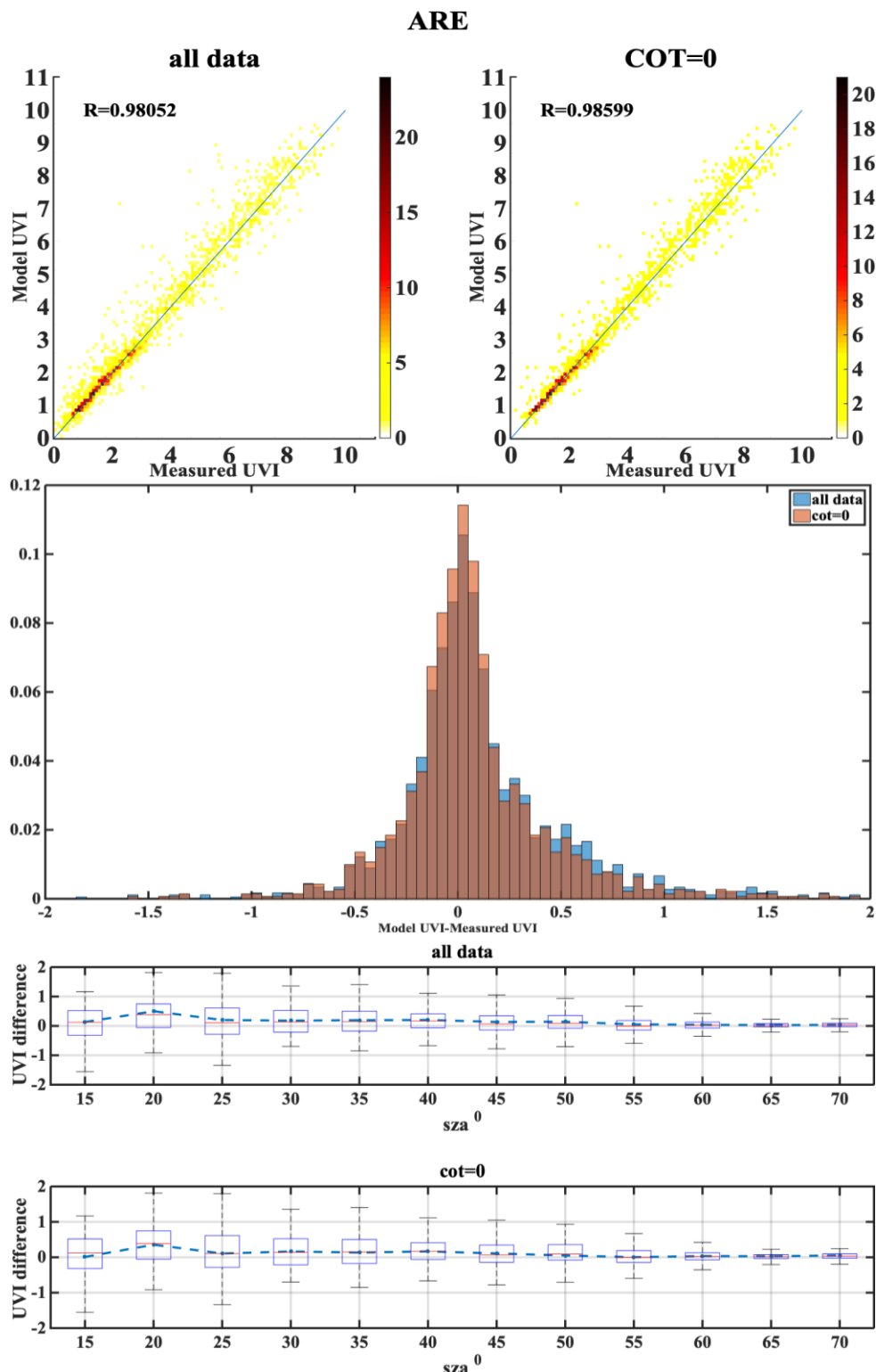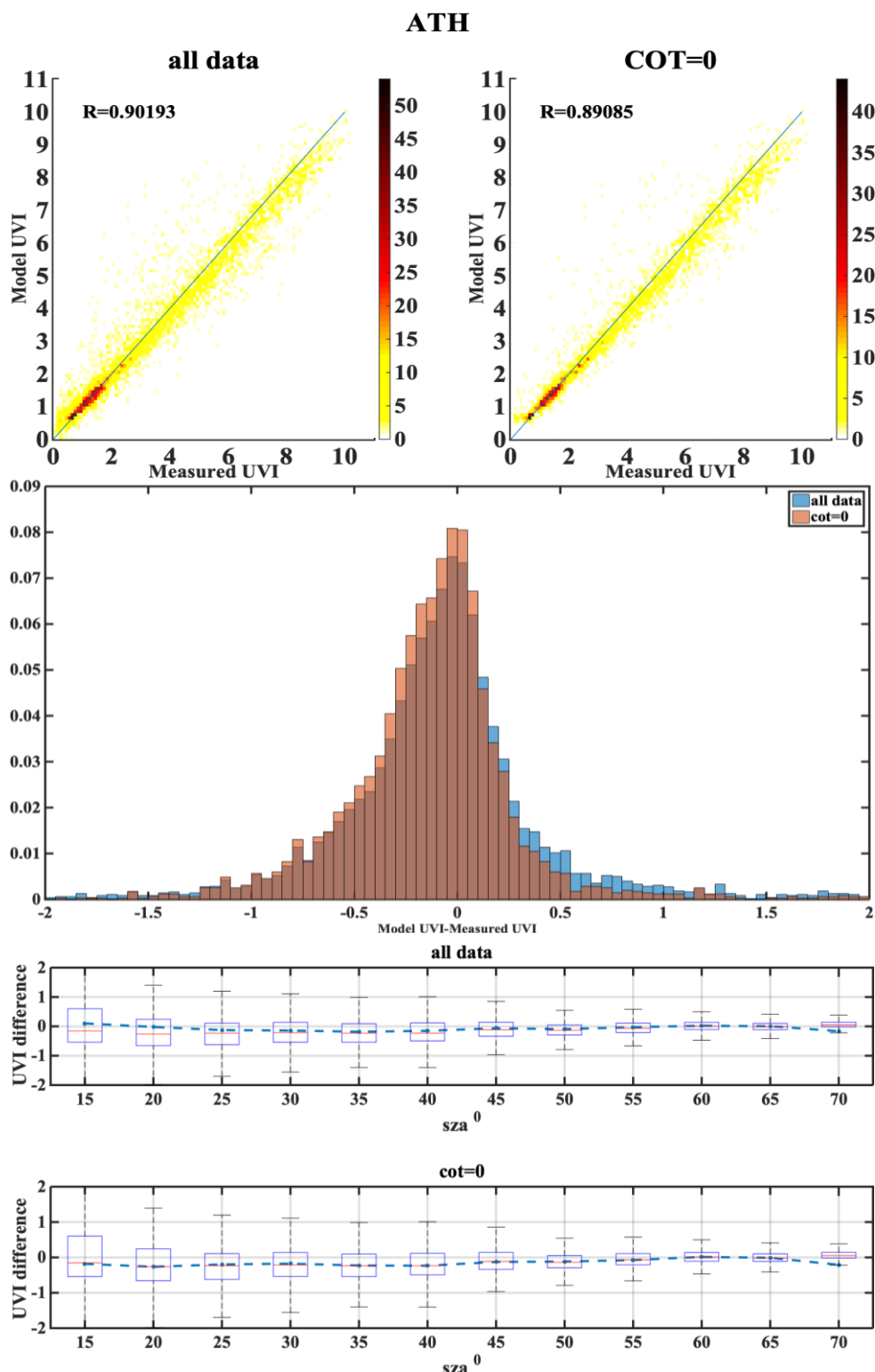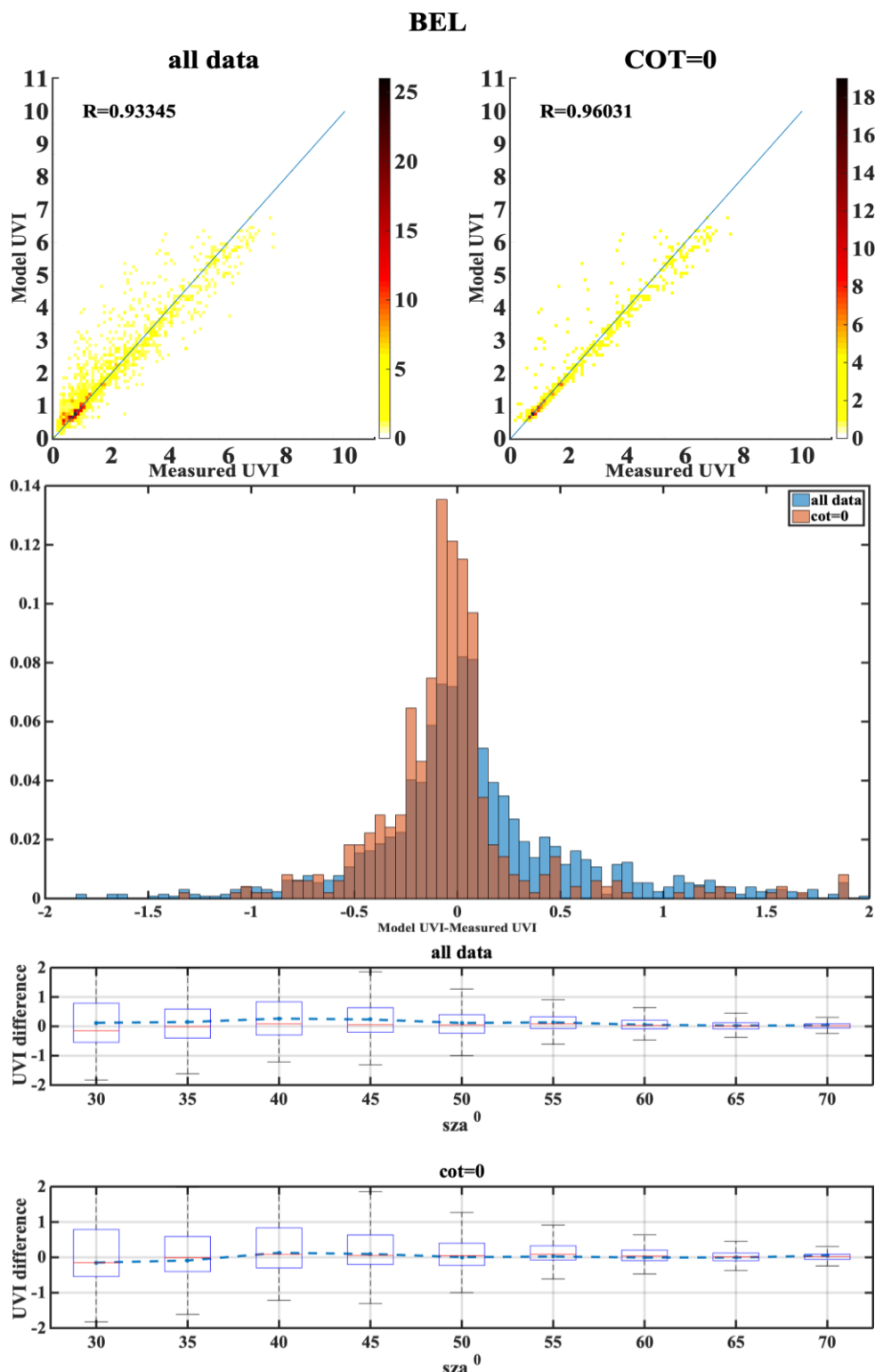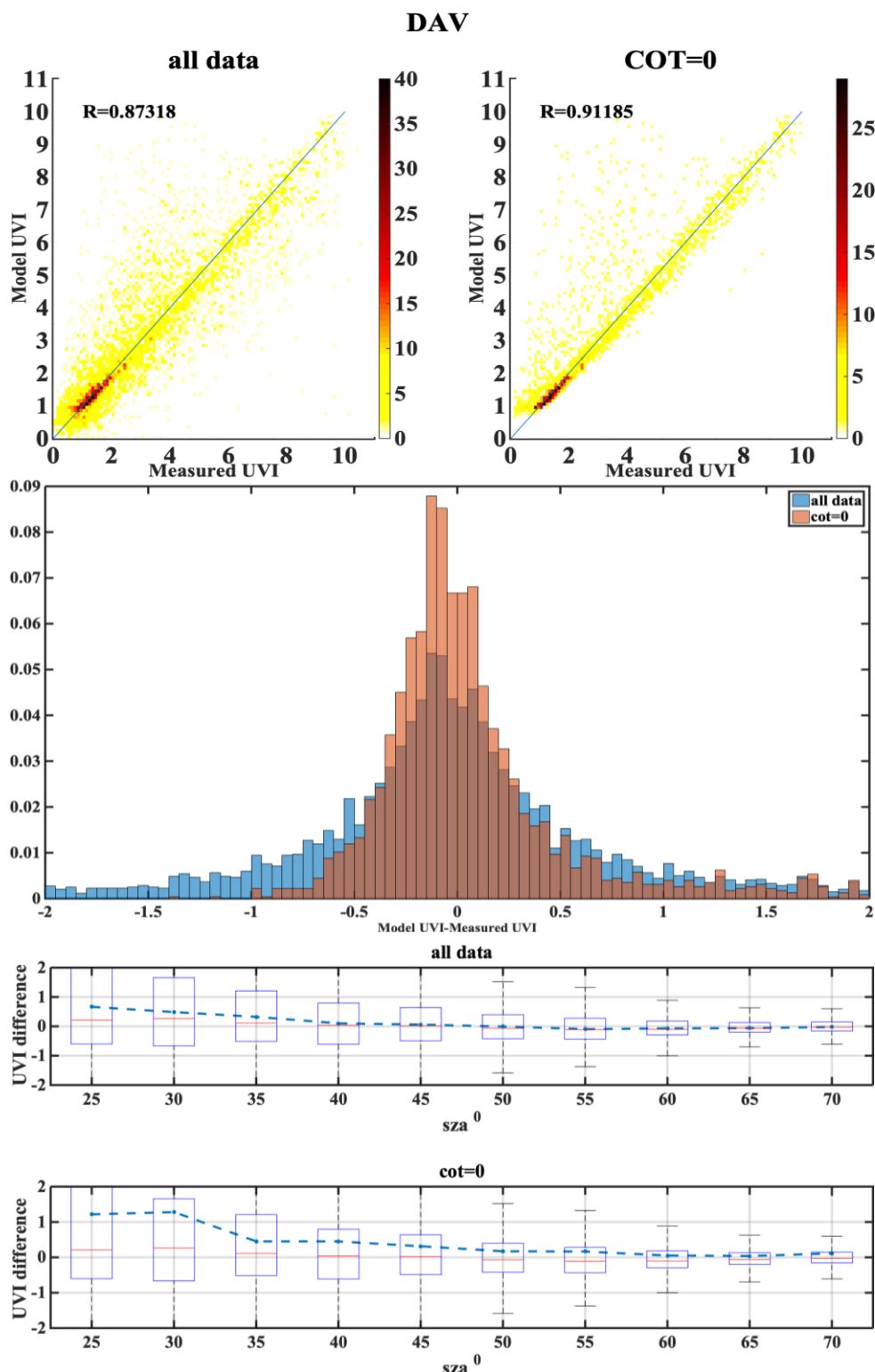| Station	All data	Data COT=0
AKR	6547	5379
AOS	5607	3551
ARE	1814	1414
ATH	4892	3548
BEL	1317	505
DAV	5635	2410
HEL	595	255
INN	4365	1919
LAN	7409	3302
LIN	3795	1387
MAN	7854	1946
ROM	1532	1196
SOD	860	269
THE	9750	6867
UCC	3007	983
VAL	9795	6497
VIE	4199	2094

1358
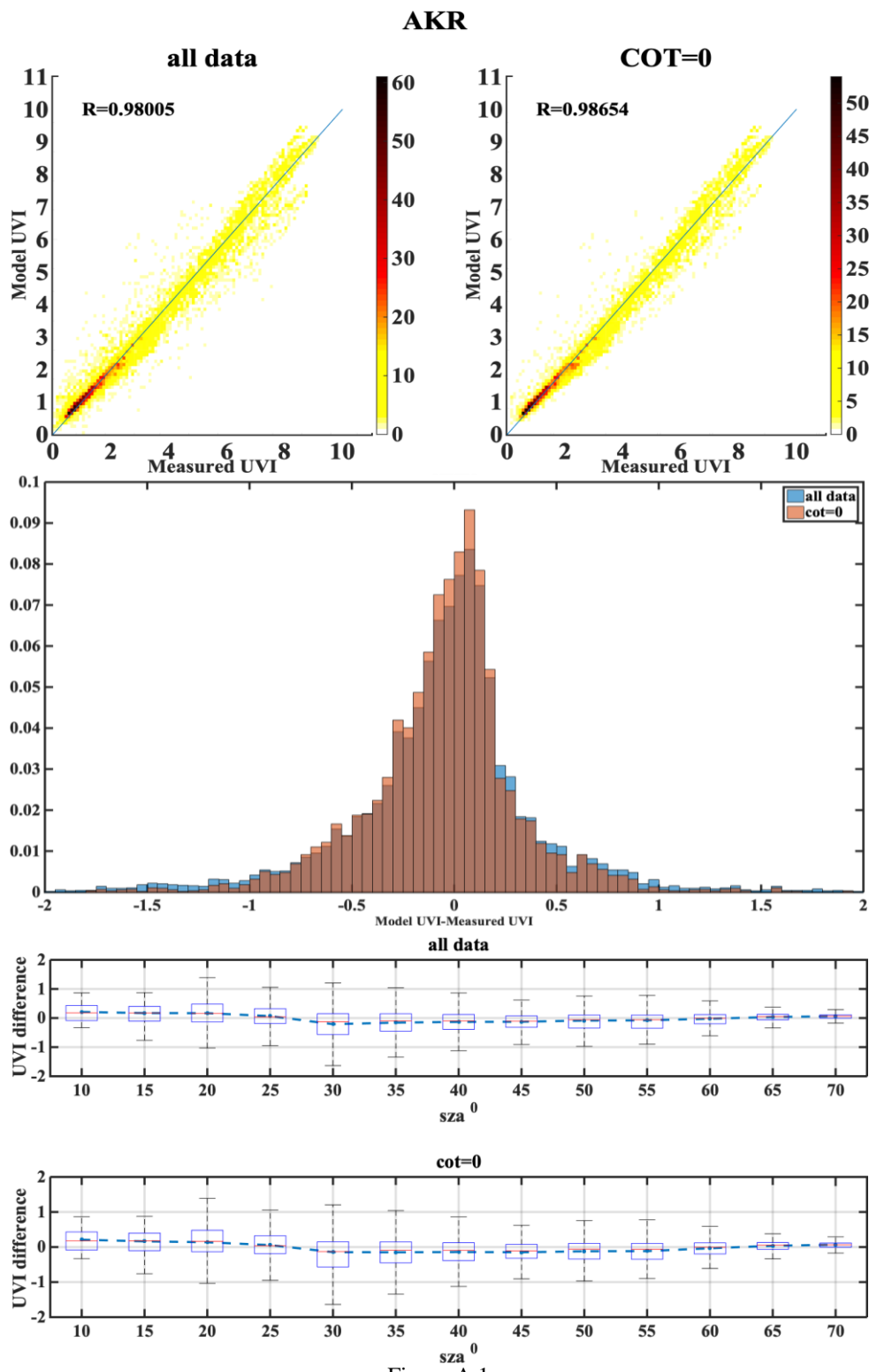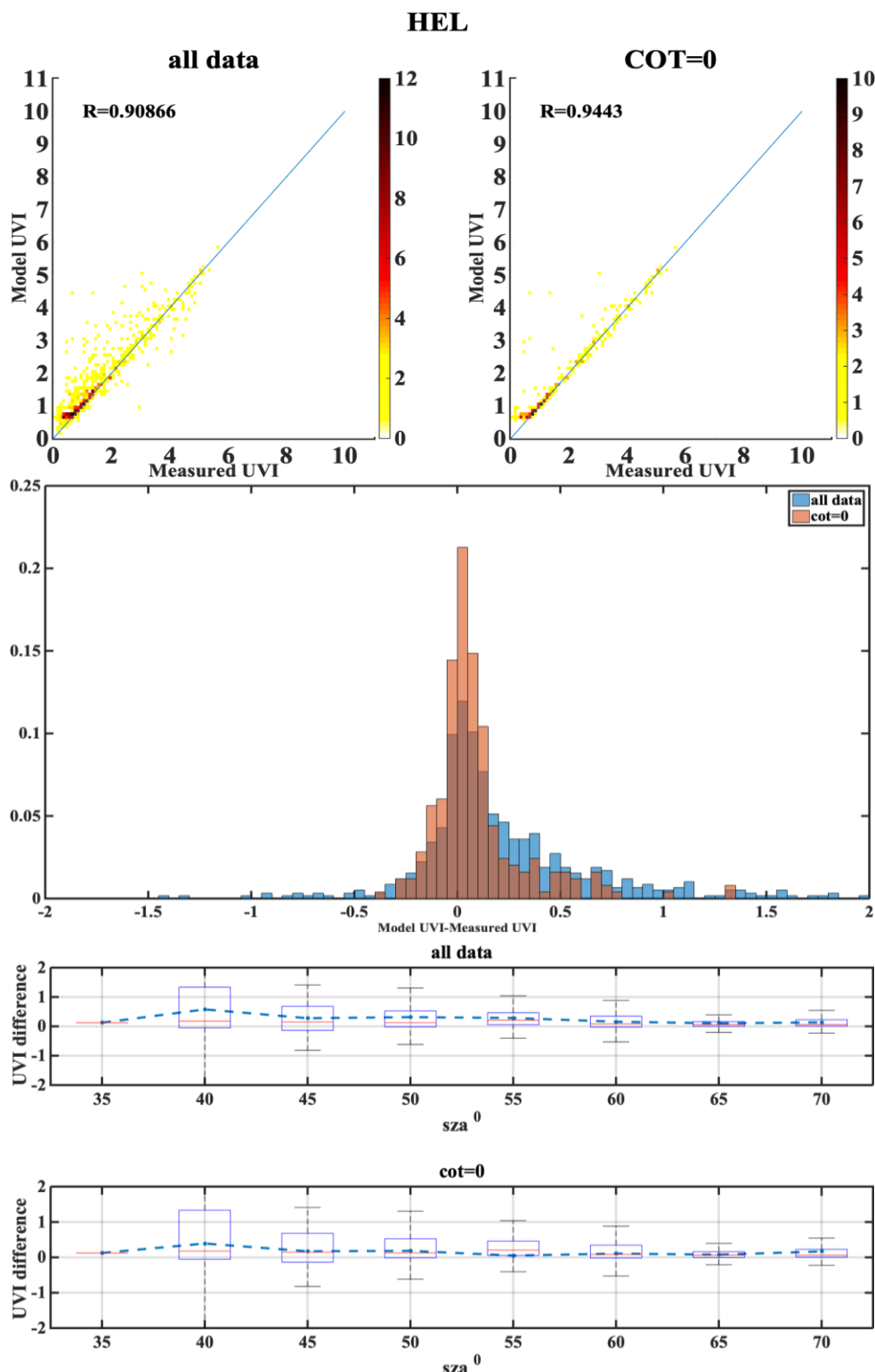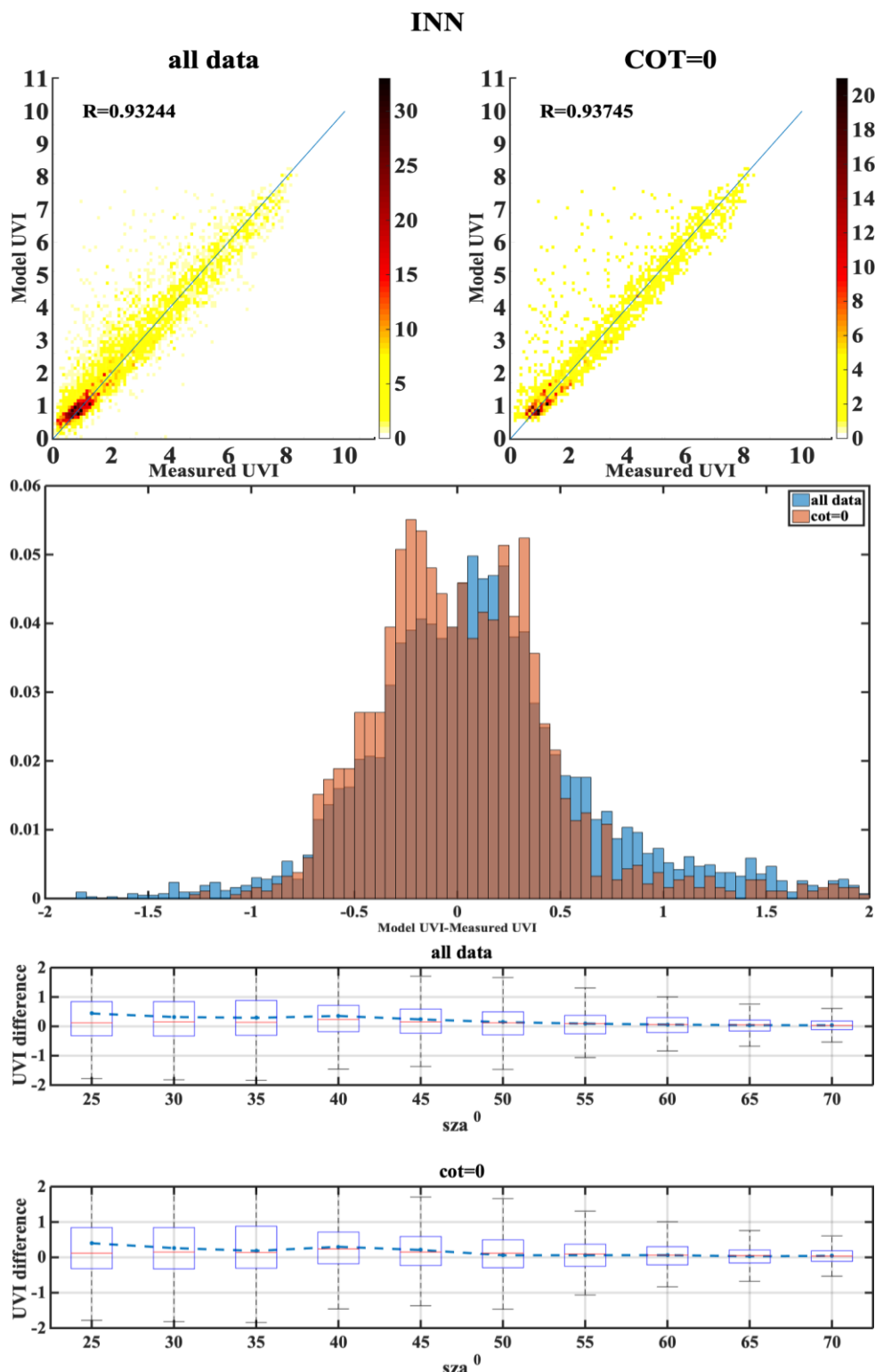
Figure A.1

Figure A.2

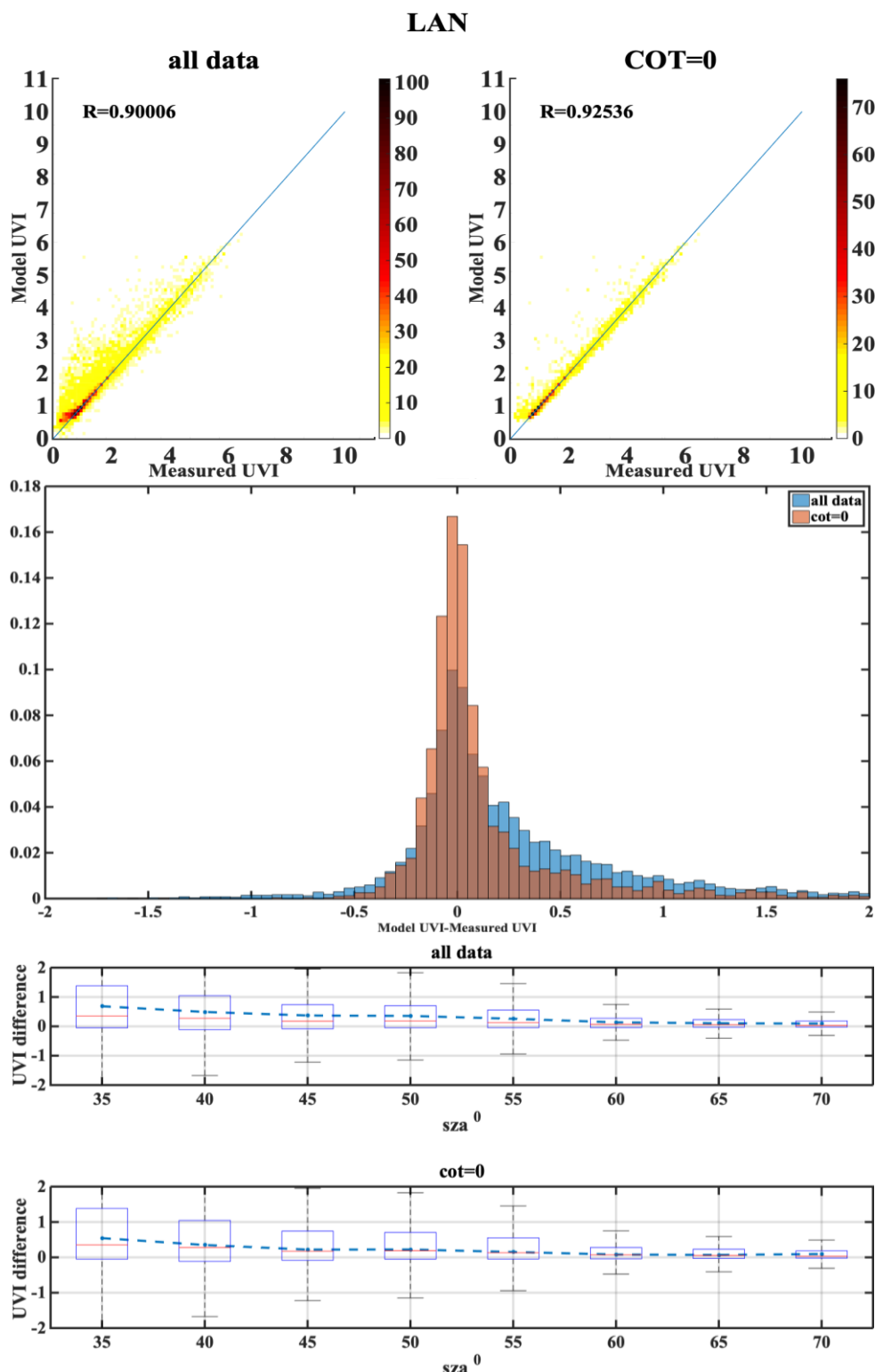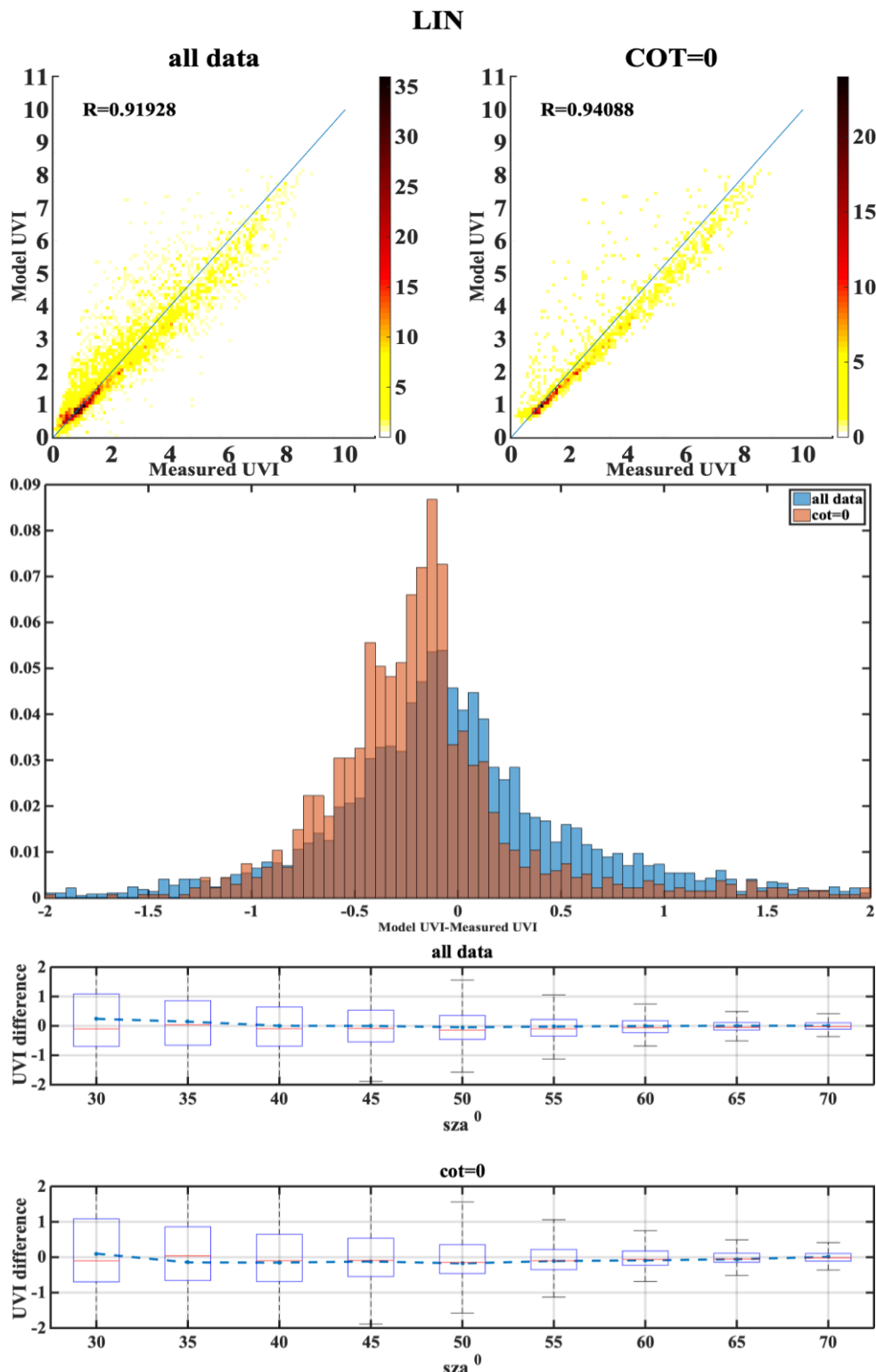Figure A.3

Figure A.4

Figure A.5
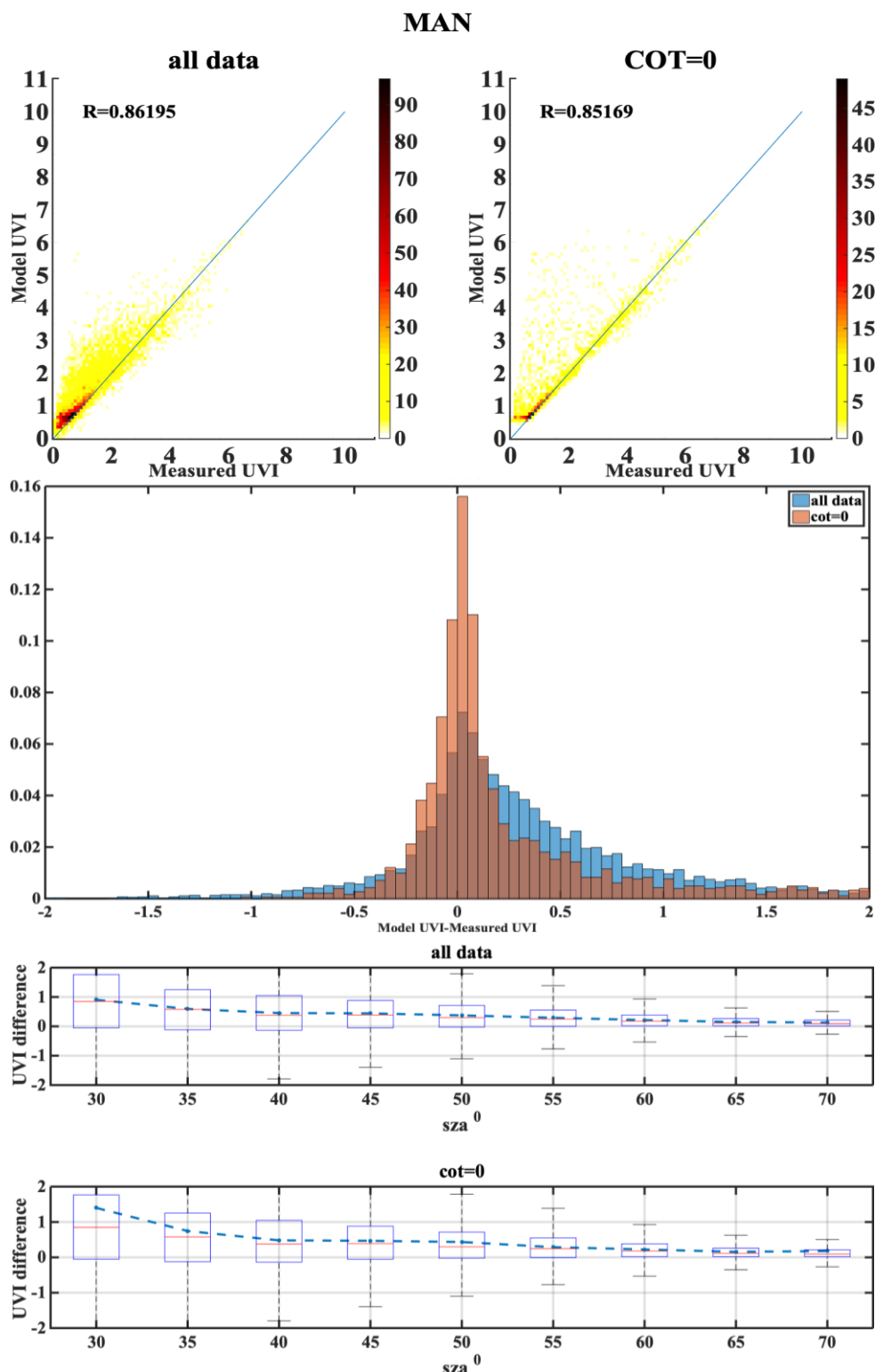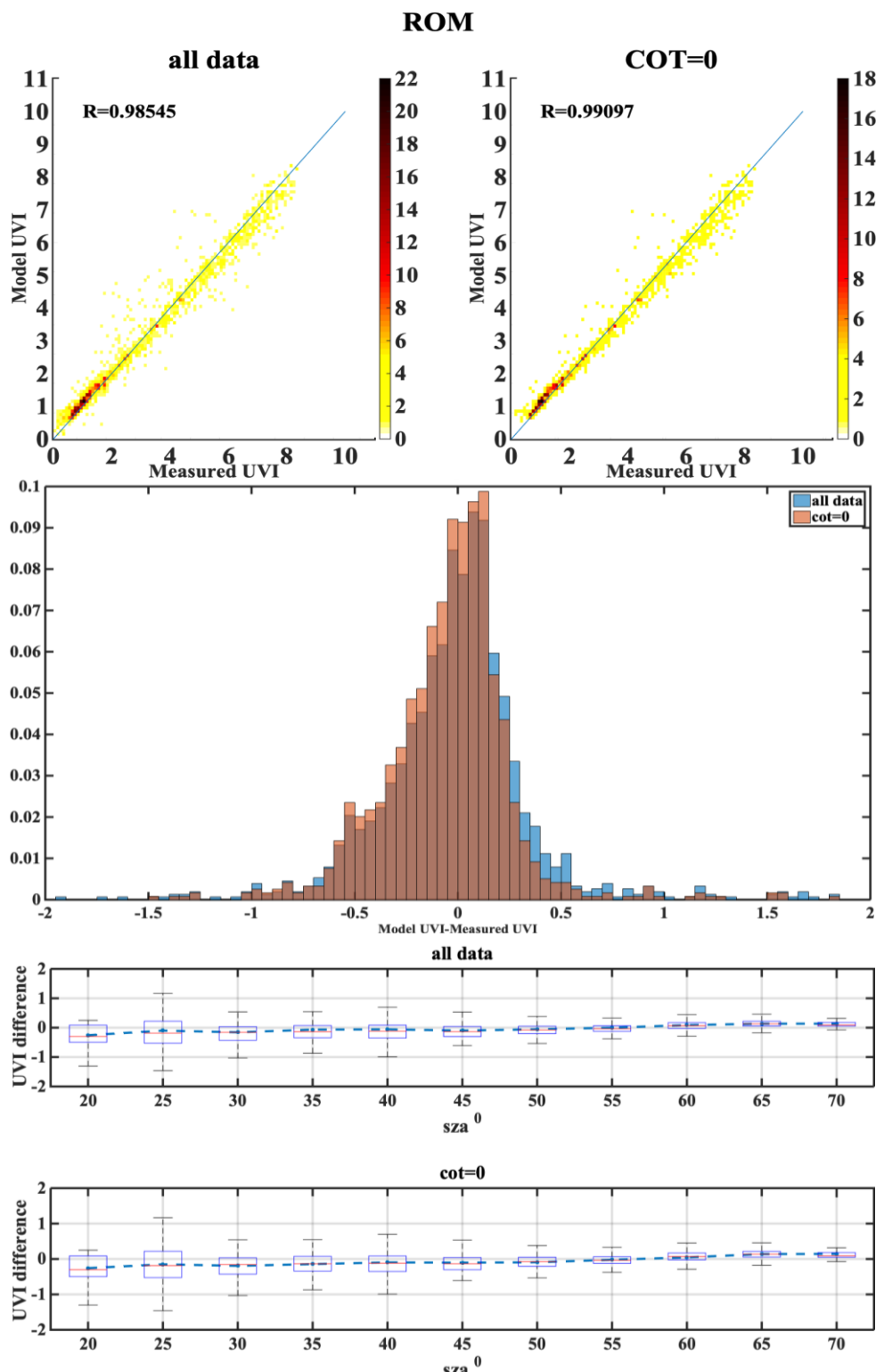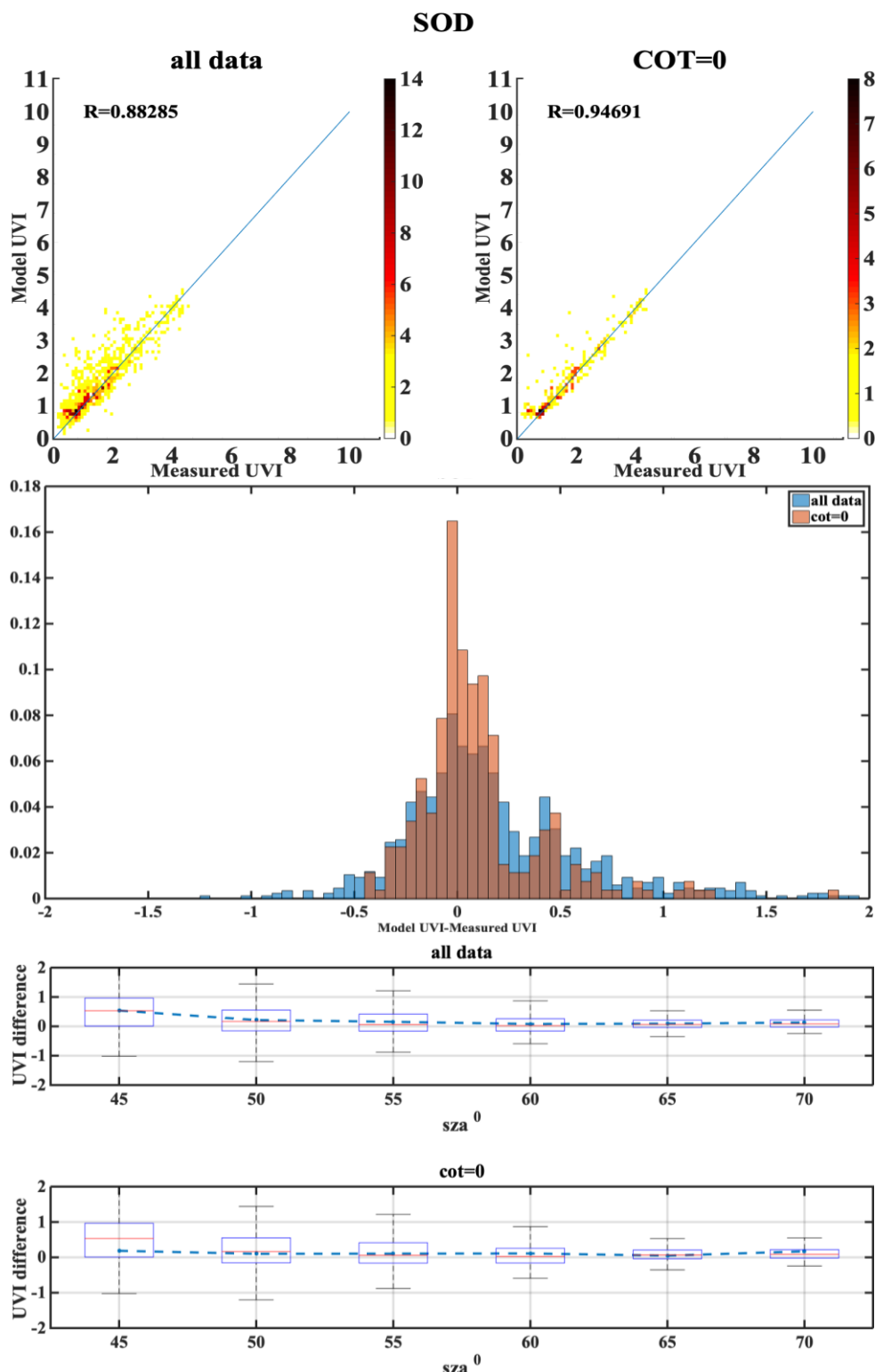
Figure A.6

Figure A.7

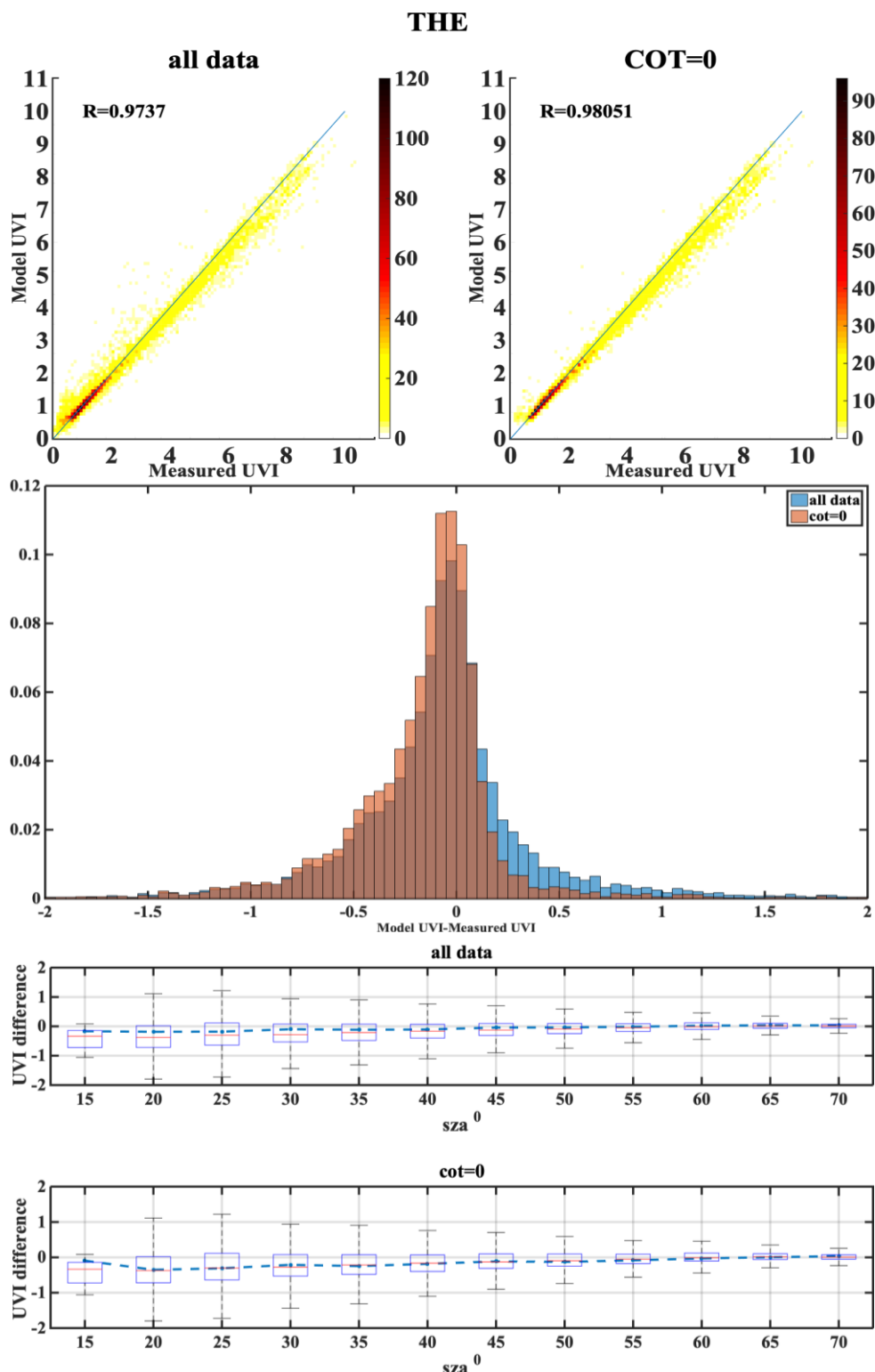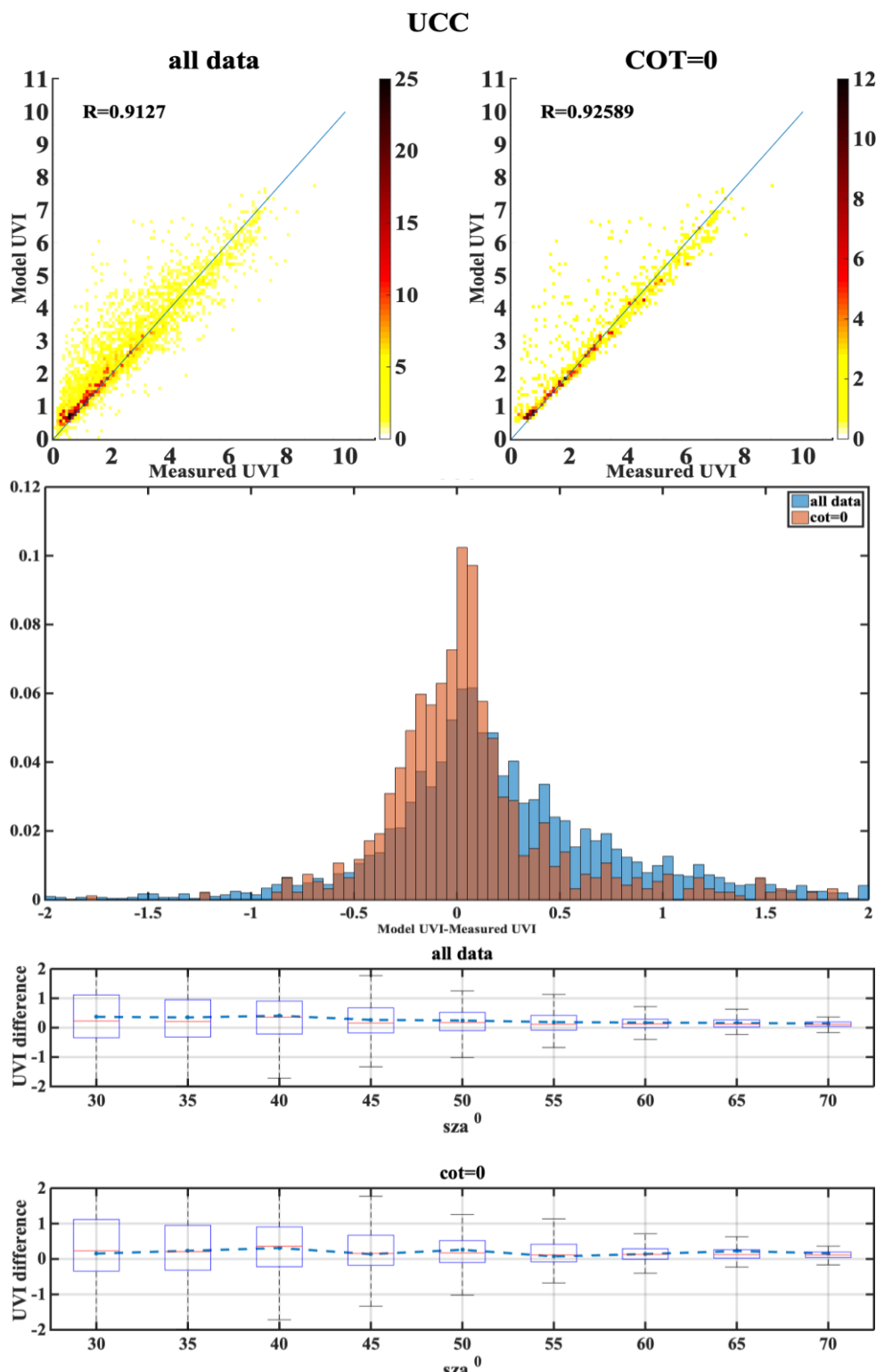Figure A.8

Figure A.9
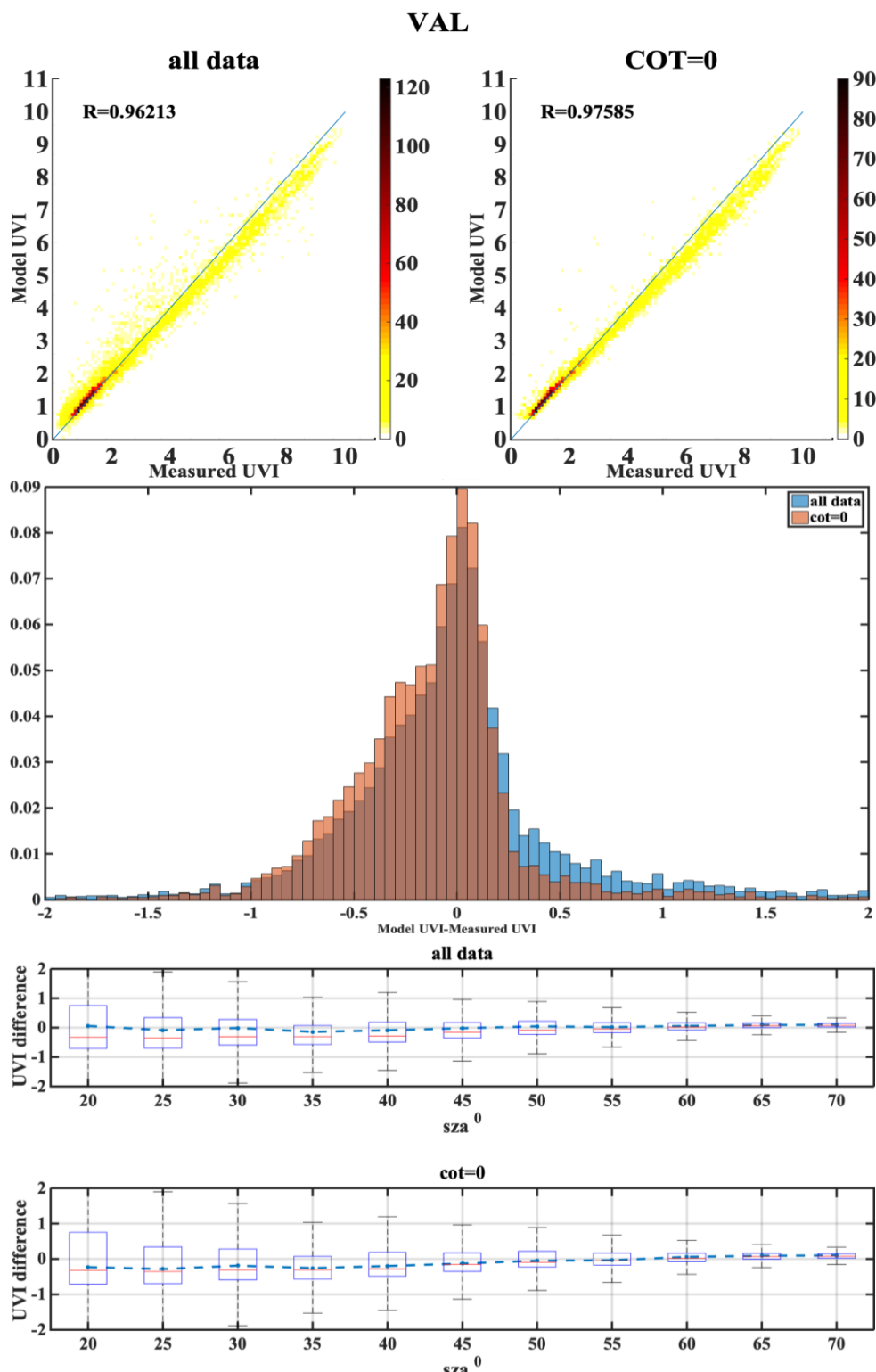
Figure A.10
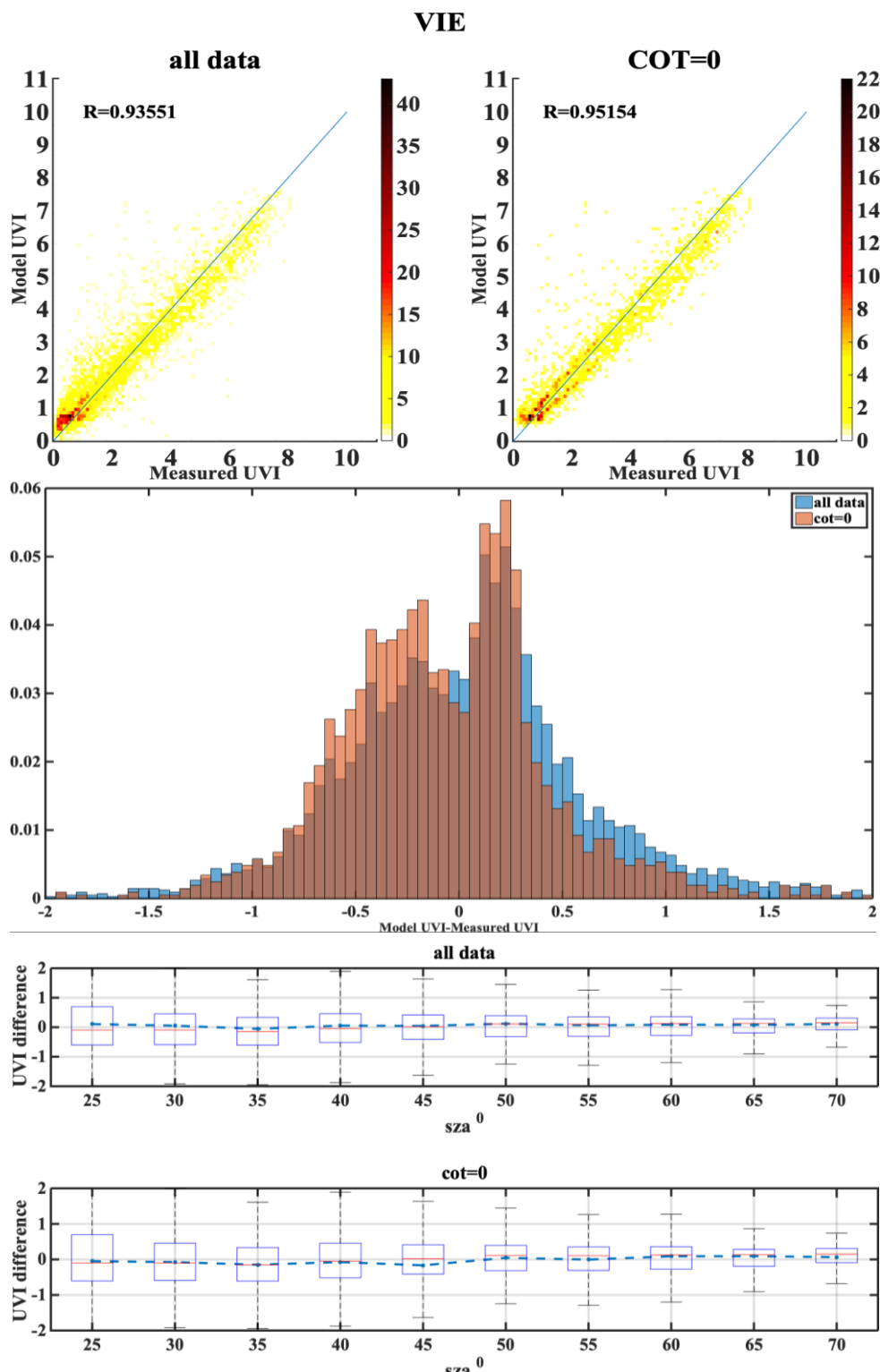
Figure A.11

Figure A.12

Figure A.13

Figure A.14

Figure A.15

Figure A.16

Figure A.17

1359